

PREPRINT

Author-formatted, not peer-reviewed document posted on 29/04/2026

DOI: <https://doi.org/10.3897/arphapreprints.e197459>

**Tectonics of the Mont Tendre and Mont Risoux (Internal
Jura Mountains): mapping and 2D kinematic forward
modelling**

 **Jon Mosar, Anina Ursprung**

1 Tectonics of the Mont Tendre and Mont Risoux (Internal Jura Mountains): mapping and 2D

2 kinematic forward modelling

3

4 Anina Ursprung¹ and Jon Mosar²

5 ¹ Federal Office of Topography swisstopo, Swiss Geological Survey, Seftigenstrasse 264, 3084 Wabern,

6 Switzerland, anina.ursprung@swisstopo.ch

7 ² corresponding author: Department of Geosciences, University of Fribourg, Chemin du Musée 6, 1700

8 Fribourg, Switzerland, jon.mosar@unifr.ch

9

10 Abstract

11 This study focuses on a new geological cross-section and forward model of the Mont Tendre and Mont
12 Risoux anticlines within the Internal Jura of the Jura fold-and-thrust belt. The results are based on
13 fieldwork, remote sensing, data compilation of previous studies and geological maps.

14 We propose a refined understanding of the wedge geometry, especially the near top basement surface.

15 We identify a large-scale structural unit with an important along-strike continuity, formed by the main
16 regional Vallée de la Saine thrust. This thrust has a 15 km long flat in the Cretaceous units and

17 accommodates a displacement of 17 km, which lead to the formation of the Mont Risoux nappe. The

18 importance of major thrusting in the clay-rich Middle Cretaceous series is recognised as a corollary of

19 the structural modelling. The interpretation of the Risoux-1 deep well has led to the determination of

20 the significant secondary décollement levels in the clay-rich Lower to Middle Jurassic series that lead

21 to the formation of important flats, fishtail and pop-up geometries in structurally higher levels. The

22 activation of the Vallée de Joux frontal thrust resulted in the formation of the Mont Tendre anticline,

23 which lead to the dissection of the Mont Risoux nappe into a sub-unit in the SE, the Mont Tendre

24 nappe. The formation of the Vallée de Joux thrust was followed by a backstepping sequence and a

25 locally oscillating thrust sequence. This detailed interpretation of the sequential development,

26 highlighting the importance of top to the south thrusting (backthrusting), confirms the mechanics of a
27 low-tapered wedge with the décollement in the weak evaporites promoting backthrusting. Moreover,
28 the tectonic nappes demonstrate the lateral structural subdivision by primary thrusts, which have a
29 NE-SW orientation, and by the primary strike-slip faults, which have a NNW-SSE and ESE-WNW
30 orientation. We propose a kinematically viable solution for the activation of the Vallée de la Saine thrust
31 and the formation of the Mont Tendre anticline, which were active between 14 Ma and 4 Ma and
32 accommodated a shortening of some 20 km.

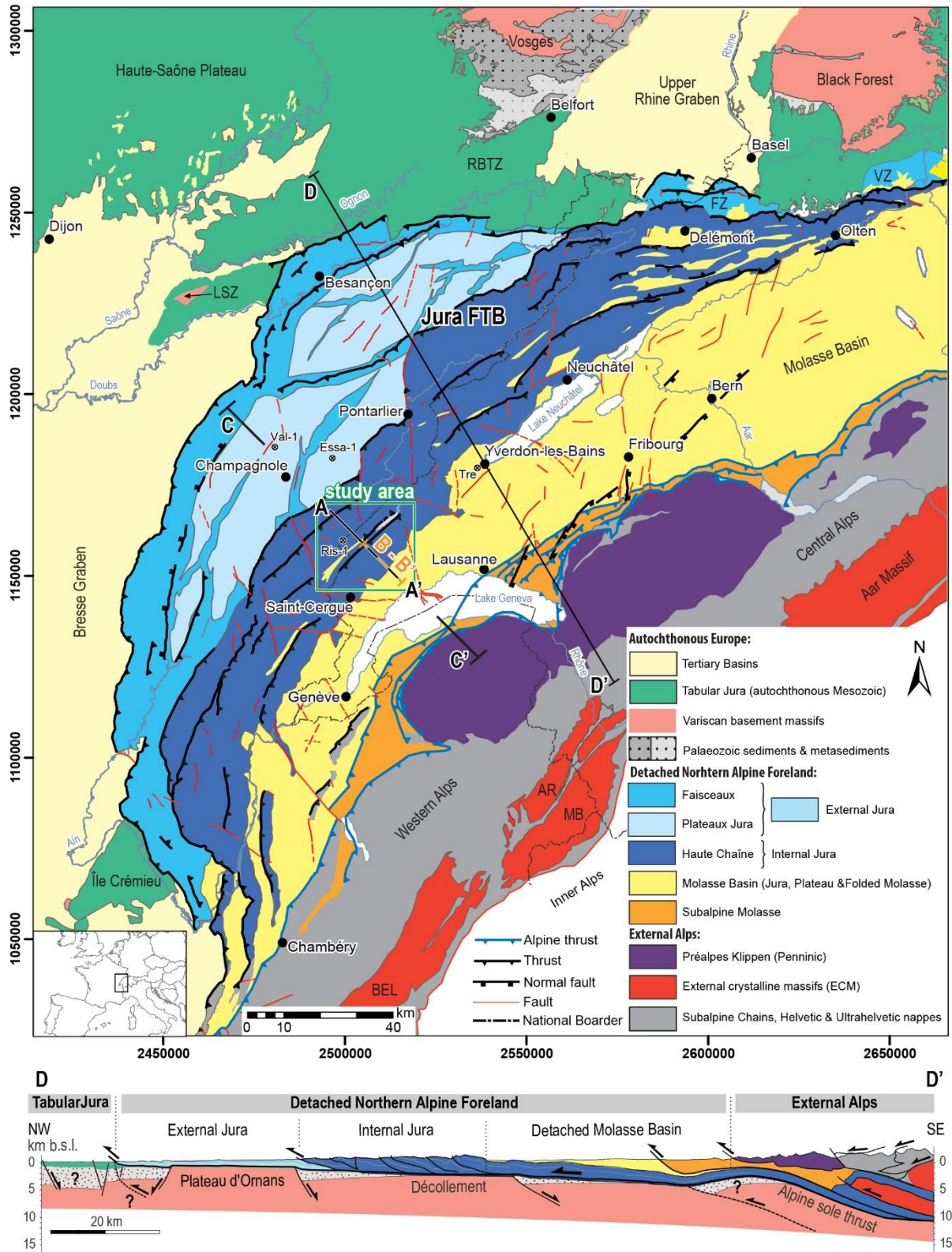
33

34 **Keywords:** Jura fold-and-thrust belt, 2D forward modelling, balanced cross-section, Mont Tendre, Mont
35 Risoux, Risoux-1 deep well, tectonic nappes, backthrusting wedge, pop-up geometry

36

37 1 Introduction

38 The Jura Mountains are a crescent-shaped fold-and-thrust belt (FTB) located in the northwestern
39 foreland of the Western Alpine arc of Europe. They form the outermost frontal part of the Alpine
40 orogenic wedge and extend from Southern Germany to Northern Switzerland and Eastern France (Davis
41 and Engelder 1985; Sommaruga 1997; Burkhard and Sommaruga 1998; Mosar 1999; Schori 2021;
42 Mosar et al. 2025b). The western border of the Jura FTB is defined by its thrust over the Bresse Graben
43 rift shoulder. To the north, it thrusts onto the autochthonous Tabular Jura as well as into the Upper
44 Rhine Graben. The Jura FTB terminates in the south, where it merges with the Subalpine Chains (Deville
45 et al. 1994; Deville and Sassi 2006; Deville 2021). The southeastern limit and the easternmost part of
46 the Jura FTB are defined by the erosive limit with the Northern Alpine Foreland Basin (NAFB), the
47 Molasse Basin (DeCelles and Giles 1996; Sommaruga et al. 2017; Schori 2021) (figure 1).



48
 49 **Figure 1:** Tectonic overview map of the Alpine Mountain range, the detached Northern Alpine Foreland, the
 50 autochthonous Tabular Jura and the Tertiary Basins, stretching from southern Germany, north-west of
 51 Switzerland to south-east of France (modified after Schori 2021). The cross-section D – D' from the External Alps
 52 to the Tabular Jura Mountains represents the tectonics of the Northern Alpine Foreland Basin (NAFB) in section

53 view (adjusted after Sommaruga et al. 2017; Schori 2021). The geological cross-section of this study corresponds
54 to section A – A' and the forward modelled cross-section of this study is the section B – B'. The study area is
55 indicated by the green rectangle that corresponds to the map extract of the local geological map (figure 4). The
56 cross-section C – C' represents the basement geometry of this study, from the Préalpes Klippen in the southeast
57 to the most distal External Jura in the northwest. Abbreviations: AR: Aiguilles Rouges Massif, BEL: Belledonne
58 Massif, FZ: Ferrette Zone, LSZ: La Serre Zone, MB: Mont Blanc Massif, RBTZ: Rhine Bresse Transfer Zone, VZ:
59 Vorfaltenzone.

60

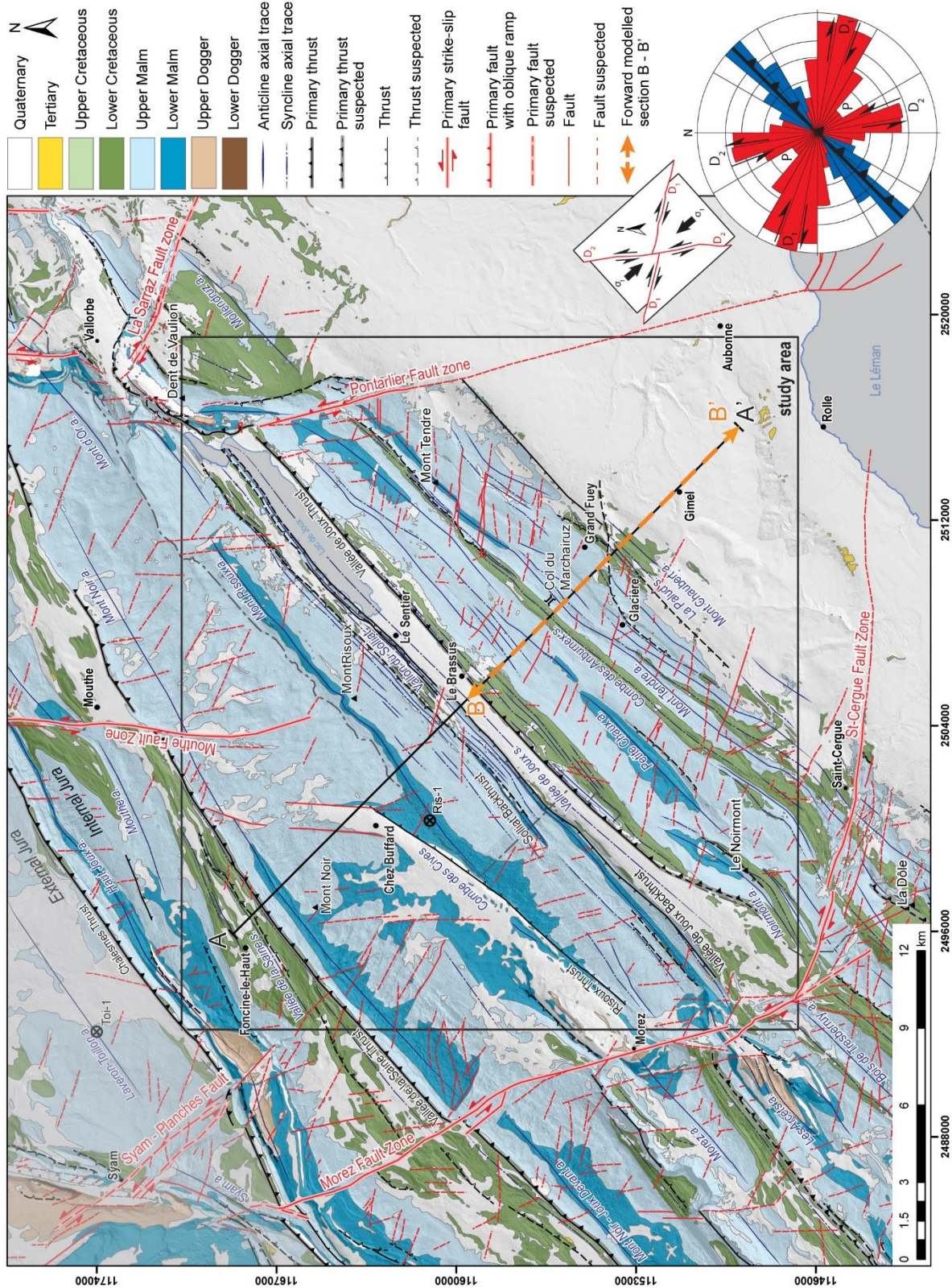
61 The study area is situated in the tectonic unit of the Internal Jura, also referred to as the Haute Chaîne,
62 and lies geographically in the Canton of Vaud in Western Switzerland and in the Jura Department in
63 Eastern France. The 26 km long cross-section A – A' extends from the Swiss Plateau across the Col de
64 Marchairuz (1'447 m a.s.l.) to the Vallée de Joux, a north-east oriented topographically high valley
65 (1'024 m a.s.l.), and over the Mont Risoux (1'384 m a.s.l.) and Mont Noir (1'234 m a.s.l.) to Foncine-le-
66 Haut in the Vallée de la Saine in France (figure 2). The profile crosses thus in its southern portion the
67 topographically prominent Mont Tendre anticline (1'679 m a.s.l.), which is the highest summit of the
68 Swiss Jura Mountains.

69 Numerous previous studies (e.g. Buxtorf 1906; Laubscher 1961; Sommaruga et al. 2017) have
70 demonstrated that the Jura FTB is detached from its substratum along a basal décollement level hosted
71 in the Triassic salt-rich evaporitic series, namely the salt series of the Keuper Group in the study area.
72 The underlying Muschelkalk Group and the Buntsandstein are then considered part of the mechanical
73 basement (see also Sommaruga et al. 2017; Marro et al. 2023). The Mesozoic to Cenozoic cover
74 sequence was thus detached from its mechanically rigid substratum and was deformed by thrusting
75 and thrust-related folding. The typical thrust geometries encountered are ramps and flats, blind
76 thrusts, fish tail geometries and backthrusts, which root within the Triassic evaporites of the basal
77 décollement level. The Jura FTB deformation style is defined as thin-skinned deformation within a

78 mechanical wedge (Davis and Engelder 1985), which implies no deformation of the mechanical
79 basement (Buxtorf 1907; Laubscher 1961; Burkhard and Sommaruga 1998).

80

81 The objectives of this study are to elucidate the structural development and kinematics of the Mont
82 Tendre anticline s.l., and its position in the larger tectonic frame. The Mont Tendre anticline s.l. is
83 defined as the large-scale complex structure between the Molasse Basin and the Vallée de Joux
84 syncline. The focus is particularly on the fold development resulting from a dominant top-to-south
85 directed thrusting. Since this significant regional structure is located at the transition of the Molasse
86 Basin and the Internal Jura, it is crucial to assess the position of the near-top basement geometry. To
87 this end, we constructed the geological cross-section A – A' to assess the surface and subsurface
88 geology on a regional scale. Balanced and kinematic forward modelling was used to further investigate
89 the structural style of the Mont Tendre anticline s.l. and the Vallée de Joux syncline (section B – B'). The
90 geological cross-section A – A' of the Mont Risoux anticline s.l., which is defined as the large-scale
91 structure between the Vallée de Joux syncline and the Vallée de la Saine syncline, was used to embed
92 our forward model in a regional setting and to better constrain the subsurface geology. The final cross-
93 section proposed in this study yields the amount of shortening and kinematic sequence of the folds
94 and thrusts on a regional scale. It also proposes a new interpretation in terms of the tectonic nappes,
95 discussing the large Mont Risoux nappe, which includes the sub-unit of the smaller Mont Tendre, which
96 is thrust on top of the Chalesmes nappe in the NW.



97

98 **Figure 2:** Regional tectonic map of the Central Internal Jura, projected in the CH1903+ / LV95 coordinate system.

99 The cross-section of this study is from A to A' and the forward modelled cross-section of this study from B to B'.

100 The geology of Switzerland corresponds to the Geological Atlas of Switzerland by swisstopo and the geology of

101 France to the geological department maps (BD Charm-50) by InfoTerre BRGM. The hillshades come from

102 swissALTI3D 5 m by swisstopo in Switzerland and from RGE ALTI 5 m by the IGN in France. The fold axial traces
103 link the folds, thrusts and strike-slip faults on a local scale (modified after Schori 2021). The faults and thrusts
104 within the study area are analysed by the rose diagram, which illustrates the distribution of the azimuth of the
105 faults (in red) and thrust axes (in blue). The rose diagram is created in MOVE by the SCAT function. An interval
106 size of 10 is used and the data are represented in a bidirectional diagram type. The rose diagram is contextualised
107 with the schematic illustration of a conjugate fault system observed in laboratory experiments (modified after
108 Burg 2018).

109

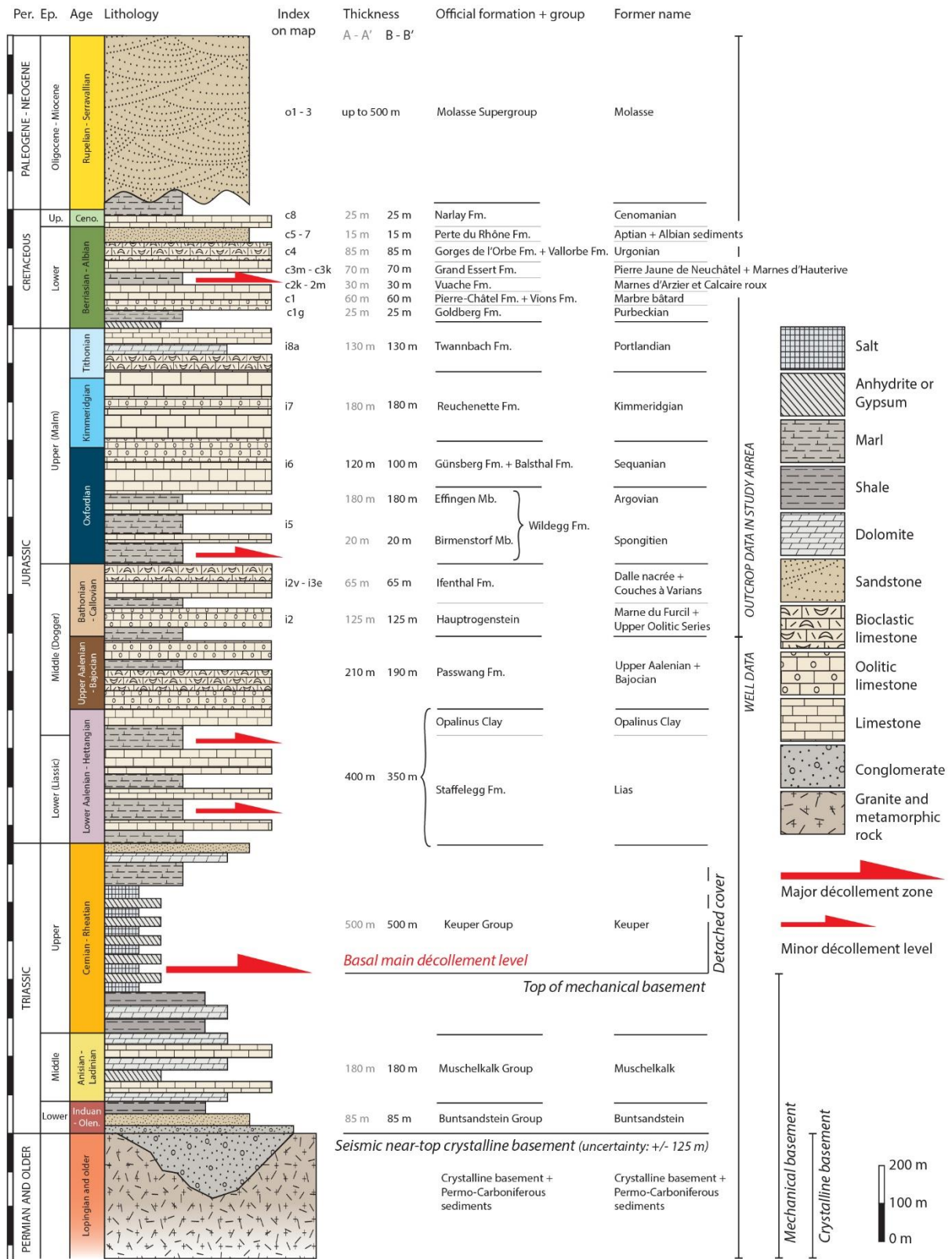
110 2 Stratigraphy

111 The Jura FTB lithostratigraphy consists of a pre-Mesozoic crystalline basement and Permo-
112 Carboniferous sedimentary rocks, and a Mesozoic and Cenozoic sedimentary cover (figure 3).
113 Subsurface data from the crystalline basement to the Lower Dogger Group were described in several
114 deep boreholes, including Essavilly-1, Valempoulières-1 and Treycovagnes-1 (see figure 1 for their
115 locations). The sedimentary rocks from the Upper Dogger Group to the most recent Quaternary
116 deposits outcrop in the study area. They are described in Aubert (1941), Sommaruga (1997), Rime et
117 al. (2019) and the Lithostratigraphic Lexicon of Switzerland (www.strati.ch).

118 The crystalline basement consists of granites and metamorphic rocks mostly associated with the
119 Variscan orogeny. These outcrop in the Vosges, the Black Forest Massif, the La Serre Zone and the
120 External Crystalline Massifs (ECM) (figure 1). Local half-grabens formed in the crystalline basement
121 during the Permo-Carboniferous period as a result of the post-Variscan extensional phase (Schori 2021;
122 Madritsch et al. 2024). The Permo-Carboniferous sediments deposited in the half-grabens, as well as
123 on and beyond the rift shoulder, consist of red shales, sandstones, silts, conglomerates and breccias.
124 At the beginning of the Mesozoic era, the early Triassic sediments were deposited in an epicontinental
125 to continental, shallow marine environment on the post-Variscan peneplain. These sedimentary rocks
126 of the Buntsandstein Group, which comprise of colourful sandstones and conglomerates, were
127 deposited on inherited topography resulting amongst other from older half-grabens and provide the

128 main setting for the present near-top mechanical basement surface (figure 3). The Muschelkalk Group
129 is made up of limestones, dolomites, and an evaporitic series of salt, anhydrite and gypsum. The Keuper
130 Group is composed of another evaporitic series and limestone. The Keuper Group evaporites, with a
131 thickness of up to 500 m, are the mechanically weak zone hosting the main basal décollement. The
132 Lower Jurassic Staffelegg Formation and the Middle Jurassic Opalinus Clay series are low energy,
133 shallow basin deposits and consists of marls, silty to sandy limestones. They may host secondary
134 detachment levels (Schori et al. 2015; Nussbaum et al. 2017; Rime et al. 2019). During the Middle
135 Jurassic, the depositional environment changed to a shallow, low-energy marine platform. The
136 Passwang Formation consists of oolitic and marly limestones. Similar oolitic limestones with marly
137 alternations are also present in the Hauptrogenstein series. The Ifenthal Formation consists of marly
138 limestones and is rich in crinoid fragments. The Wildegg Formation of the Upper Jurassic is divided into
139 two members: the Birmenstorf Member and the Effingen Member. It consists of limestones with
140 alternating marly layers and may host secondary detachment levels (Nussbaum et al. 2017). The
141 Günsberg, Balsthal, Reuchenette and Twannbach Formations were deposited in a shallow marine
142 environment. They consist of massive, pure to marly and dolomitic limestones (Sommaruga 1997). The
143 sedimentary rocks from the Early Cretaceous period comprise oolitic, bioclastic and marly limestones
144 and evaporites. They were deposited in shallow waters of a neritic environment and may host
145 secondary detachment levels (Nussbaum et al. 2017; Rime et al. 2019). Towards the end of the Lower
146 Cretaceous and during the Upper Cretaceous, the continental influence increased, leading to the
147 deposition of sandstones, claystones, sparitic and chalky limestones. The Tertiary sediments of the
148 Molasse Supergroup are Rupelian (Oligocene) and Burdigalian (Miocene) in age. They were deposited
149 on an erosional unconformity at the top of the Mesozoic sediment and consist of sandstones,
150 conglomerates, marls and claystones. They mostly rest on the Cretaceous series and very locally on
151 Jurassic series, such as in the SW corner of our study area on the NW slope of the Vallée de Joux
152 syncline, thus suggesting the existence of preexisting relief. The Quaternary sediments, which are the
153 most recent deposits, represent only a very thin and discontinuous veneer of deposits and are not

154 further considered in this study (Aubert 1941; Sommaruga 1997; Kuhlemann and Kempf 2002; Pfiffner
 155 et al. 2002; Sommaruga et al. 2012; Rime et al. 2019).



156

157 **Figure 3:** Lithostratigraphic column of the central Internal Jura. The top of pre-Mesozoic rocks forms the near-top
 158 basement as defined from seismic interpretations with an uncertainty range of +/- 125 m (Marro et al. 2023). The
 159 basement of pre-Mesozoic age plus the in-situ sedimentary rocks of the Buntsandstein Group, Muschelkalk Group
 160 and Lower Keuper Group beneath the basal main décollement level define what we refer to the mechanical
 161 basement. Each geological age is indicated with the index number (modified after Aubert 1941), the official
 162 Formation + group (www.strati.ch), the former common name (Aubert 1941; www.strati.ch) and the thicknesses
 163 used for the geological cross-section A – A' and forward modelled section B – B'. The thicknesses for the
 164 Buntsandstein Group, Muschelkalk Group, Keuper Group, Staffelegg Formation, Opalinus Clay and Wildegg
 165 Formation are taken from the geological thickness model by Schori (2021). The thickness of the Passwang
 166 Formation comes from Rime (2018), whereas those of the Ifenthal Formation up to and including the Perte-du-
 167 Rhône Formation are based on the studies of Aubert (1941) and on www.strati.ch. The thickness of the Narlay
 168 Formation is from www.strati.ch. The thickness for the Molasse Supergroup is taken from Sommaruga (1997) and
 169 Marchant (2016). Abbreviations: Ceno.: Cenomanian, Ep.: Epoch, Fm.: Formation, Olen.: Olenekian, Per.: Period,
 170 Up.: Upper.

171

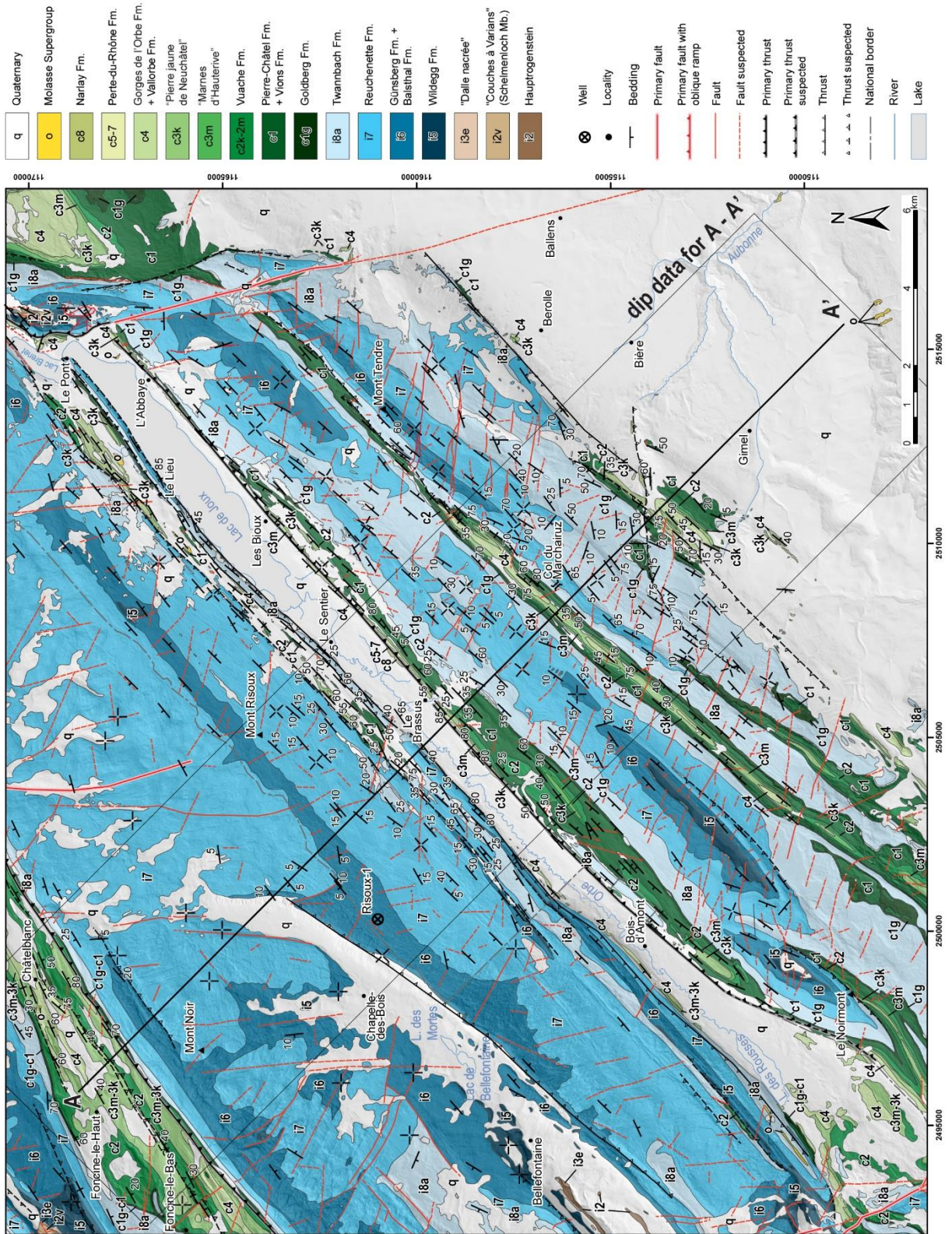
172 3 Regional tectonics

173 The NAFB and Jura FTB were detached and folded above the mechanical basement along the main
 174 basal décollement level, which lies within the Triassic evaporite series (Sommaruga et al. 2017; Schori
 175 2021; Deville 2021). Strain within the Triassic evaporites, mostly in the salt layers, is accommodated by
 176 plastic behaviour at low pressures and low temperatures, resulting in low basal friction compared to
 177 the underlying mechanical basement (Buxtorf 1907; Laubscher 1961; Jordan 1992; Gruber 2017;
 178 Sommaruga et al. 2017; Deville 2021). The strain distribution is very heterogenous with important
 179 strain partitioning. The detachment of the Northern Alpine Foreland (NAF) initiated approximately 16-
 180 14 Ma ago (Smeraglia et al. 2021). It resulted in a maximum displacement of 30 km (Buxtorf 1907;
 181 Laubscher 1961; Sommaruga 1997; Mosar 1999; Becker 2000; Kuhlemann and Kempf 2002; Pfiffner
 182 2010; Schlunegger and Mosar 2011; Sommaruga et al. 2017).

183 The basal décollement level roots beneath the ECM and outcrops at the front of the detached Northern
 184 Alpine foreland (figure 1). The northward displacement of the NAF sedimentary cover was driven by
 185 the exhumation and imbrication of the ECM basement nappes, the so-called “Fernschub” (Buxtorf
 186 1907; Laubscher 1961). The exhumation is related to the convergence of the European and Adriatic
 187 plates, which resulted in crustal shortening and the development of antiformal stacks within the
 188 crystalline substratum (Buxtorf 1916; Boyer and Elliott 1982; Burkhard and Sommaruga 1998; Homberg
 189 et al. 1999; Homberg et al. 2002; Pfiffner 2010; Schlunegger and Mosar 2011; Sommaruga et al. 2017).
 190 The ongoing orogenic growth resulted in the emplacement of a foreland fold-and-thrust belt that works
 191 as narrow mechanical taper geometry. Thus, the deformation in the foreland, that is the detachment
 192 and the formation of thrusts, backthrusts and folds, is driven by the necessity of the wedge to achieve
 193 equilibrium (Davis and Engelder 1985; Mosar 1999; Schlunegger and Mosar 2011; Schori 2021; Mosar
 194 et al. 2025a).

195 The Jura FTB is divided into four distinct tectonic domains. The Internal Jura; the External Jura, which
 196 contains the Plateaux and Faisceaux, and beyond the frontal thrust the Tabular Jura. The Internal Jura
 197 is the most deformed part which has on its “internal” southern side an erosive boundary with the
 198 detached NAFB. This domain thrusts northwards on top of the External Jura. The basement beneath
 199 the Internal Jura dips between 2 to 3° towards the southeast and includes basement faults interpreted
 200 from seismic lines and exploratory wells all across the Jura FTB (Schori 2021). The Internal Jura displays
 201 prominent anticlines linked to fault propagation folding and ramp-flat geometries, along with
 202 associated thrusting that has partially duplicated the Mesozoic cover. The External Jura consists of the
 203 weakly deformed Plateaux and the strongly deformed, folded Faisceaux. The Tabular Jura represents
 204 the autochthonous part of the Mesozoic sedimentary cover, beyond the frontal thrust of the Jura FTB.
 205 It is characterised by steep normal faults, many of which reach into the pre-Mesozoic basement and
 206 sub-horizontal beds (Sommaruga 1997; Schori 2021). The central Jura FTB contains important strike-
 207 slip fault systems, which have a WNW-ESE and N-S orientation (Sommaruga 1997; Schori 2021) such as
 208 the Pontarlier Fault (Radaideh and Mosar 2019). They show locally a component of oblique movement.

209 The major thrusts and strike-slip zones divide the Jura laterally into distinct structural domains (figure
 210 1).



211

212 **Figure 4:** Detailed geological map of this study area, projected in the CH1903+ / LV95 coordinate system. It is the
 213 result of the compilation and harmonisation of the local lithostratigraphy (figure 3), the geological maps of the
 214 Geological Atlas of Switzerland by swisstopo and of the geological department maps (Bd Charm-50) by InfoTerre
 215 BRGM. The hillshades come from the swissALTI3D 5 m by swisstopo in Switzerland and from the RGE ALTI 5 m by
 216 the IGN in France. The section trace A – A' corresponds to the geological cross-sections of this study (figure 7, 11,
 217 12). The faults and thrusts as well as their hierarchisation are modified after Schori (2021). The suspected faults
 218 contain lineaments from Sturny (2018). The dip data are from fieldwork and of the Geological Atlas of Switzerland.

219

220 4 Methodology

221 The interpretation of the surface and subsurface geology of the study area is based on a compilation
 222 of published geological maps, the Risoux-1 deep well data and interpretation of vintage seismic profiles.
 223 The data were further densified by detailed fieldwork along the section trace in the central part of the
 224 study area. All data were implemented into a GIS system. The 2D kinematic forward modelling is based
 225 on existing modelling algorithms (MOVE 2020.1 - IPM 12.5 by Petroleum Experts).

226 4.1 Surface geology and mapping

227 The surface geology interpretation in this study is based on the geological map sheets of Cossonay
 228 (Custer and Aubert 1935), Le Sentier (Aubert 1941), Marchairuz (Falconnier 1950), Orbe (Aubert and
 229 Dreyfuss 1963) and Morges (Vemet 1972) from the 1:25'000 Geological Atlas of Switzerland published
 230 by swisstopo. The geological maps of the Doubs and Jura departments, by the BRGM, cover the study
 231 area in France. The detailed geological map shows the official lithostratigraphic Formations and Groups
 232 (figures 3, 4; www.strati.ch), which have been grouped together according to their respective epochs
 233 on the regional tectonic map (figure 2). Hillshades cast shadows onto the topography, allowing
 234 geological structures such as faults and thrusts to be easily identified on a 2D map. This allows local
 235 surface geology to be studied using remote sensing in GIS (Schori 2014). Switzerland is covered by
 236 swissALTI3D (swisstopo 2011), whereas France is covered by RGE ALTI® (IGN-F 2018). The dataset for
 237 the thrusts and faults is a compilation of Schori (2021) and the Geological Atlas of Switzerland by

238 swisstopo. The dip data are shown on the detailed geological map, with a higher density of data
239 acquired during fieldwork, near the cross-section. The dip data considered for the construction of the
240 surface geology are within the black rectangle in figure 4. Dip data combined with a new analysis of the
241 structures seen on the hillshade, made it possible to draw the refined position of the fold axial traces
242 on the regional tectonic map and thus highlight the link between folds, thrusts, and strike-slip faults on
243 a local scale.

244 4.2 Risoux-1 deep well and seismic data

245 The Risoux-1 deep well is located on the Mont Risoux anticline, 2.3 km west of our cross-section. It is
246 the oldest deep well within the Jura FTB (Winnock 1961) and provided the first evidence for the
247 existence of thrusts and repetitions of the Mesozoic cover series in the Jura FTB (Sommaruga 1997).
248 The well has a final depth of 1'958 meters below the surface (appendix 1). The following thrusts are
249 described from bottom to top of the well: At 1'660 meters below the surface, there is a minor intra-
250 Malm thrust (Wildegge Formation) showing no significant displacement. At 1'234 meters below the
251 surface, the main regional thrust causes the Liassic units (Staffelegg Formation and Opalinus Clay) to
252 be thrust on top of the Malm units (Günsberg Formation and Balsthal Formation). The thrust at 975
253 meters below the surface, within the Liassic units (Staffelegg Formation and Opalinus Clay), is
254 considered here as a secondary intra-clay detachment level. Intra-Dogger thrust (Passwang Formation,
255 Hauptrogenstein and Ifenthal Formation) and intra-Malm thrust (Wildegge Formation) of minor
256 importance are identified at depths of 643 meters and 478 meters below the surface, respectively.
257 Another secondary detachment level, thrusting the Dogger units (Passwang Formation and
258 Hauptrogenstein) on top of the Malm unit (Wildegge Formation), is described at a depth of 453 meters
259 below the surface (appendix 1).

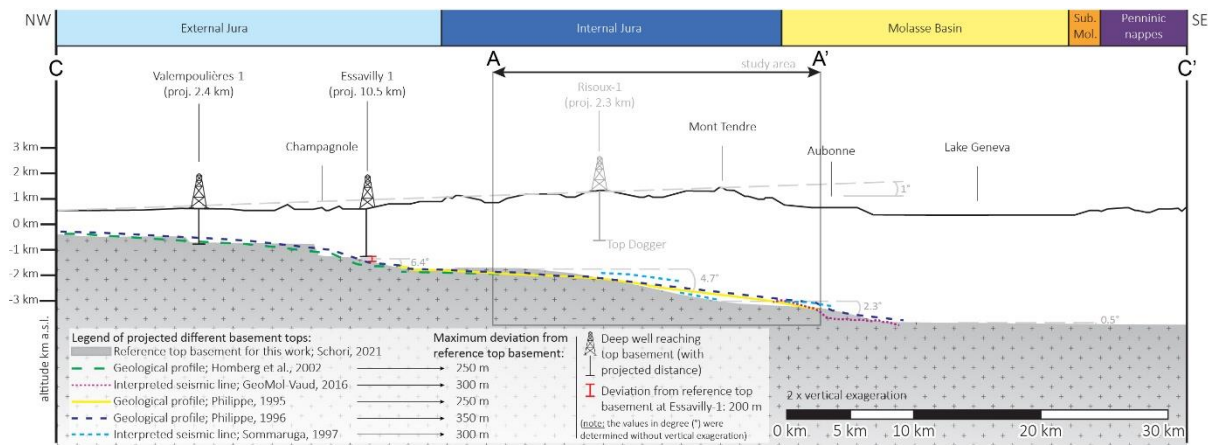
260 The seismic surveys conducted in the vicinity of the study area between 1972-1974 and in 1976, include
261 three seismic profiles (73-VD-25, 72-MAR-2 and 74-VD-76) oriented in the dip direction, which were
262 interpreted in two-way-travel time (TWT) by Sommaruga (1997) and converted to depth by Marchant
263 (2016) (figure 5). These data are used to support the interpretation of the Risoux-1 deep well. Sub-

268 **Figure 5:** The seismic lines 74-VD-46, 72-MAR-2, 73-VD2-25 (a) along with their interpretations (b) projected onto
 269 the cross-section of this study A – A'. The basis of cross-section A – A' corresponds to the base of the Mesozoic
 270 cover by Schori (2021). The coloured lines represent the seismic horizons and faults, which were interpreted by
 271 Sommaruga (1997). The map extract shows the localization of the seismic lines (c).

272

273 4.3 Basement geometry

274 The base of the Mesozoic cover is an uneven surface due to faulting within the crystalline pre-Mesozoic
 275 basement, post-Variscan erosion and the irregular deposition of Permo-Carboniferous sediments on
 276 top of pre-Mesozoic rocks, as well as in numerous graben structures. The depth of the near-top
 277 crystalline basement is determined by the geological thickness model of the base Mesozoic cover by
 278 Schori (2021), which is based on wells, cross-sections and seismic profiles that reach the top of the
 279 crystalline basement. Other published interpretations are also consistent with this model (figure 6).
 280 The crystalline basement in this study dips at an angle of 3.2° - 6.6° towards the south and reaches a
 281 depth of approximately 3'500 m below sea level beneath Lake Geneva (Schori 2021). As the lower
 282 boundary of the cross-sections A – A' and B – B' corresponds to the near-base of the detached Mesozoic
 283 cover, within an uncertainty range, which in turn corresponds to the top of the mechanical basement,
 284 the geological thickness models of the Buntsandstein Group and Muschelkalk Group by Schori (2021)
 285 are added on top of the crystalline pre-Mesozoic basement. Forward modelling in Move with a unique
 286 dip makes modelling much easier, as no fault-related folds should form in the deeper part of the
 287 section. Therefore, an angle with a single dip of 3.5° has been defined based on the average inclination
 288 across the modelled section B – B'.



289

290 **Figure 6:** Presentation of the different interpretations of the top crystalline basements and projected wells. The
 291 grey area represents the top crystalline basement chosen for this study (Schori 2021). This section C – C' extends
 292 from the Préalpes Klippen to the most distal External Jura. The locations of the represented wells are indicated
 293 in figure 1. The geological cross-section of this study A – A' is highlighted with a rectangle and arrows. The vertical
 294 scale has been exaggerated by a factor of 2 to enhance the visibility of the differences in height between the
 295 various interpretations.

296

297 4.4 Construction of the geological cross-section A – A'

298 The surface geology of the geological cross-section A – A' was constructed based on field observations
 299 (particularly bedding dip measurements) and geological information from the geological and tectonic
 300 maps (figure 2, 4). The surface interpretation extends to a depth of approximately 300 - 500 meters
 301 below the surface and comprises near-surface folds and thrusts. To construct the subsurface structures
 302 covering the area below the surface geology, down to the crystalline basement, we used the
 303 interpreted seismic lines (Sommaruga 1997), the description of the Risoux-1 well (Winnock 1961) and
 304 the position of the near-top crystalline basement (Schori 2021). The position of the Vallée de Joux
 305 thrust and the presence of the Top Keuper unit beneath the Mont Tendre anticline s.l. are based on
 306 seismic interpretations and are important for constructing the southern part of the cross-section. The
 307 positions of the Top Dogger and Top Keuper units as interpreted in the seismic data, differ from those
 308 shown in the geological cross-section A – A'. This is because constant stratigraphic thicknesses were

309 used (figure 3) and because the deep structural interpretation must be linked to the structural style of
 310 the surface geology observed in the field. The large backthrust identified in the seismic interpretation
 311 at a depth of 1'550 meters below the surface, to the southeast of the Risoux-1 well, aligns with the
 312 minor intra-Malm thrust described in the Risoux-1 well at a depth of 1'660 meters below the surface,
 313 considering the projection of the seismic and well data onto the geological cross-section (figure 5,
 314 appendix 1). The description of the Risoux-1 deep well shows a main vertical displacement of 1'350
 315 meters at a depth of 1'234 meters below the surface. We therefore identified this significant thrust as
 316 the main regional thrust in the study area (Vallée de la Saine thrust) and reinterpreted the large
 317 backthrust shown in the seismic interpretation as a minor intra-Malm thrust (figure 7). The
 318 discontinuous seismic reflectors beneath the Vallée de Joux syncline, in the footwall of the Vallée de la
 319 Saine thrust, form an antiformal bulge in the Mesozoic units resulting from a Keuper duplex at the basal
 320 décollement level. The interpreted seismic horizons from the Top Muschelkalk to the Top Malm units
 321 are continuous and horizontal to the north and south of this bulge (figure 5, 7).

322 4.5 2D kinematic forward modelling of the section B – B'

323 The 2D kinematic forward modelled section B – B' was constructed using the software MOVE by
 324 Petroleum Experts with the implemented 2D Move-on-Fault module. The model deforms rocks in the
 325 hanging walls of faults, while the beds in the footwall remain unaffected by deformation and do not
 326 undergo translation. The forward kinematic modelling involved iterations of tests to unravel the initial
 327 geometry or single faults modelled individually step by step. The aim of the forward model is to yield
 328 the deformation of an undeformed layer cake along predefined activated fault systems. Input from a
 329 regional balanced section and all available data help to constrain a series of iterations of intermediate
 330 solutions until a final model reaches the present-day structures observed in the field (Endignoux and
 331 Mugnier 1990). To ensure that the forward model is also kinematically balanced, the area of the
 332 transferred and deformed mass has to be preserved across the two-dimensional cross-section (Hossack
 333 1979; Endignoux and Mugnier 1990; Fossen 2010), the stratigraphic thickness has to be preserved
 334 (Goguel 1952; Endignoux and Mugnier 1990), the model considers thrusts systems with ramp and flat

335 geometries deforming the bedding in the hangingwall to generate folds, which may suffer subsequent
336 deformations (Boyer and Elliot 1982; Endignoux and Mugnier 1990) and only one fault can be active at
337 a single step (Mitra 1986; Endignoux and Mugnier 1990).

338 The forward model of the study was constructed in MOVE, using the stratigraphic thickness indicated
339 in figure 3 as B – B'. The following method algorithms were incorporated: Fault Parallel Flow (FPF), Fault
340 Bend Fold (FBF), Trishear and Wedge modelling. FPF assumes translation parallel to complex fault
341 geometries such as steeply dipping fold limbs (Egan et al. 1997; Egan et al. 1999; Kane et al. 1997),
342 while FBF keeps the bed length constant, with translation parallel to the fault surface and is limited in
343 the software for ramps of a maximal angle of 30° (Suppe 1983). Trishear deforms sedimentary beds
344 within a triangular shear zone in front of the tip of a propagating fault (Erslev 1991). Using only FBF and
345 FPF to maintain bed thickness constant throughout our model would be too difficult and time
346 consuming to construct a viable section. The Trishear approach is used because it makes it possible to
347 find geometrically reasonable solutions. It is beyond the scope of this paper to assess the fold formation
348 mechanisms in the field to justify what type of model to use. Nevertheless, it should be noted that,
349 locally, bedding thickness may vary, and that numerous folds exhibit layer parallel shear suggesting FBF
350 and FPF (flexural slip) mechanisms of formation. The differences in bedding thickness are, on regional
351 scale very modest, and below an estimated 10% error margin.

352 This study implemented the modelling of a wedge using the FBF algorithm, which displaces the hanging
353 wall towards the foreland. The transferred mass is then translated along the backthrust towards the
354 hinterland, while the backthrust itself is deformed and thrust towards the foreland. It is important
355 to note that MOVE has limitations when modelling simple backthrusts using the Trishear algorithm. To
356 overcome this shortcoming, we applied the method of Rime et al. (2019), which uses the FPF algorithm
357 to translate the sedimentary cover towards the foreland. The mass is then transferred by the same
358 displacement towards the hinterland using the Trishear algorithm. Figures 8 and 9 show the different
359 algorithms and parameters used in each of the eight modelling steps.

360

361 5 Interpretations and Results

362 The main structural features of the surface geology are analysed by stereonet projections of bedding
363 and structural data and rose diagrams to identify thrust and fracture lineaments from geological maps.
364 The sub-surface geology is constructed based on subsurface data such as seismic lines, drill hole data
365 and geometric and kinematic modelling.

366 5.1 Surface geology

367 The near surface structural style, which extends to a depth of approximately 300-500 meters below the
368 surface, is dominated by thrust-related folds, thrusts and subvertical fractures and strike-slip faults
369 (figures 2, 4, 7). The overall orientation of structures (fold axes and thrust directions) in the study area
370 is rather cylindrical and trends NE-SW, as typically seen in the Mont Chaubert and the Mont Risoux
371 anticlines (figures 2, 7a and 7b). The dip data were projected perpendicular into the cross-section of
372 this study, which runs parallel to the local transport direction of the Jura FTB. This direction is
373 considered to be perpendicular to the fold axial traces (figure 4, 7b). Due to the projection of the
374 geological structures from nearby outcrops onto the section trace, the surface geology in the cross-
375 section represents an averaged construction of the cylindrical geometry. Consequently, minor
376 discrepancies of a few hundred meters may occur between the mapped geology on section trace A –
377 A' and the geological cross-section. The cylindrical regularity is disrupted to the northeast of the study
378 area by the important sinistral Pontarlier strike-slip fault system and to the southwest by the sinistral
379 Morez-St-Cergue strike-slip fault system (figure 2, 4) (Aubert 1945; Aubert 1959; Laubscher 1965;
380 Laubscher 1972). Fractures and minor vertical faults are observed throughout the investigation area
381 and can be readily interpreted from the hillshades (figures 2, 4). The dominant WNE-ESE and NNW-SSE
382 directions, families D1 and D2 respectively, represent diagonal fractures within an NE-SW oriented fold
383 system. A third, less frequent fracture direction, NW-SE oriented fault family P, represents fractures
384 perpendicular to the fold axis. The diagonal faults are developed as conjugate faults in the fold and are

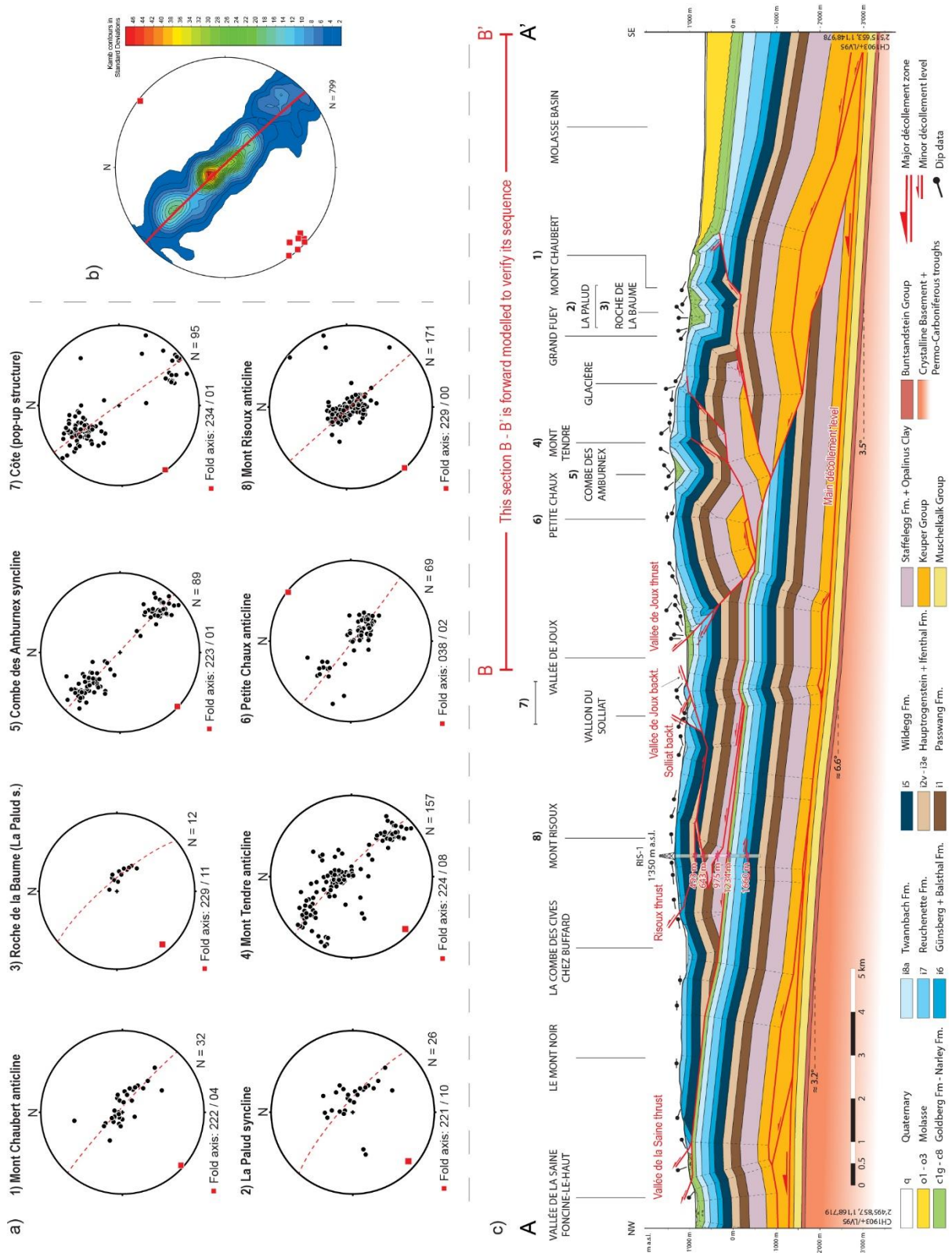
385 subsequently locally reactivated to host the major sinistral NNW-SSE strike-slip faults (e.g. Morez fault
386 zones) and the conjugate WNW-SSE dextral strike-slip faults (St-Cergue Fault Zone) (figure 2).

387 5.2 Subsurface interpretation

388 The geological cross-section (figure 7) illustrates both surface and subsurface interpretations. It is
389 important to note that the deep structural interpretations are based on surface geology, the position
390 of near-top the pre-Mesozoic crystalline basement (Schori 2021), the interpretation of the Risoux-1
391 deep well (Winnock 1961) and the interpretation of the seismic profiles by Sommaruga (1997). The
392 well and seismic interpretations were considered for the construction, but it was not possible to take
393 them fully into account.

394 The basal décollement is considered a zone of distributed deformation and is located in the Keuper
395 unit. For modelling purposes, we have positioned the décollement surface at the base of the salt rich
396 layers (figure 3). Our study reveals significant lithostratigraphic thickness variations in the Keuper
397 Group, of up to 1'000 m below the southeastern limb of the Mont Tendre anticline, which are explained
398 by the formation of duplexes (Gruber 2017; Schori 2021). The main regional thrust of the study area is
399 the Vallée de la Saine thrust, which roots below the Mont Tendre anticline and outcrops in the Vallée
400 de la Saine syncline, located 15 km to the northwest. Its very large thrust flat is located in the marly
401 units of the Vuache Formation of Cretaceous age. Thus, the thrusting of the Staffelegg Formation and
402 Opalinus Clay series results in the duplication of almost the entire Jurassic-Cretaceous cover. The
403 seismic profiles in this area suggest that the Mesozoic units beneath the Vallée de la Saine thrust are
404 parallel to the basal décollement level. The discontinuous reflections beneath the Vallée de la Saine
405 thrust are thought to be due to a duplex structure at the basal décollement level beneath the Vallée
406 de Joux syncline, which is responsible for the gentle antiformal bulge in the Vallée de la Saine thrust
407 and the Mesozoic units above it. A larger duplex at the basal décollement level beneath the Vallée de
408 la Saine syncline enables the Cretaceous units to outcrop in the same syncline (figure 7).

409 Considering that the whole Mont Risoux-Mont Tendre area has a similar structural setting and is limited
410 to the NW by the Vallée de la Saine thrust and to the NE and SW by the major strike-slip faults of
411 Pontarlier and Morez respectively, we propose that the Mont Risoux anticline s.l. together with the
412 Mont Tendre structure belong to a single tectonic Mont Risoux nappe that shows important
413 duplications of the Mesozoic cover (figure 10) (Winnock 1961; Marro et al. 2023). We thus reassess
414 and expand on the considerations proposed on the Risoux nappe tectonics in prior work (Rigassi, 1962
415 1977; Aubert 1971; Wildi et al. 1991). The duplications are explained by a secondary, intra-clay
416 detachment level in the Vuache Formation, the Staffelegg Formation and Opalinus Clay. This results in
417 the Risoux thrust, a fishtail structure, and the Vallée de Joux backthrust and Solliat backthrust, which
418 form a pop-up geometry. These structures are rooted in the Vallée de la Saine thrust (Aubert 1971).
419 The Mont Tendre anticline, formed by the Vallée de Joux thrust, is considered a sub-unit of the Mont
420 Risoux nappe, the Mont Tendre nappe (figure 10), and is characterized by a sequence of minor
421 anticlines and synclines formed by a complex backthrusting wedge linked to distinct backthrusts (figure
422 7c).



This section B - B' is forward modelled to verify its sequence

A B B'

423

424 **Figure 7:** The lower hemisphere stereoplots (Schmidt net: equal area projection) illustrate the major folds of the
 425 study area in this work (a). The black dots represent the poles to bedding planes (N = number of bedding planes).
 426 The red dashed line represents the calculated best fit profile plane, and the red rectangle represents the
 427 calculated fold axis. The trend and plunge of the fold axis are indicated below the stereoplot (Allmendinger et al.

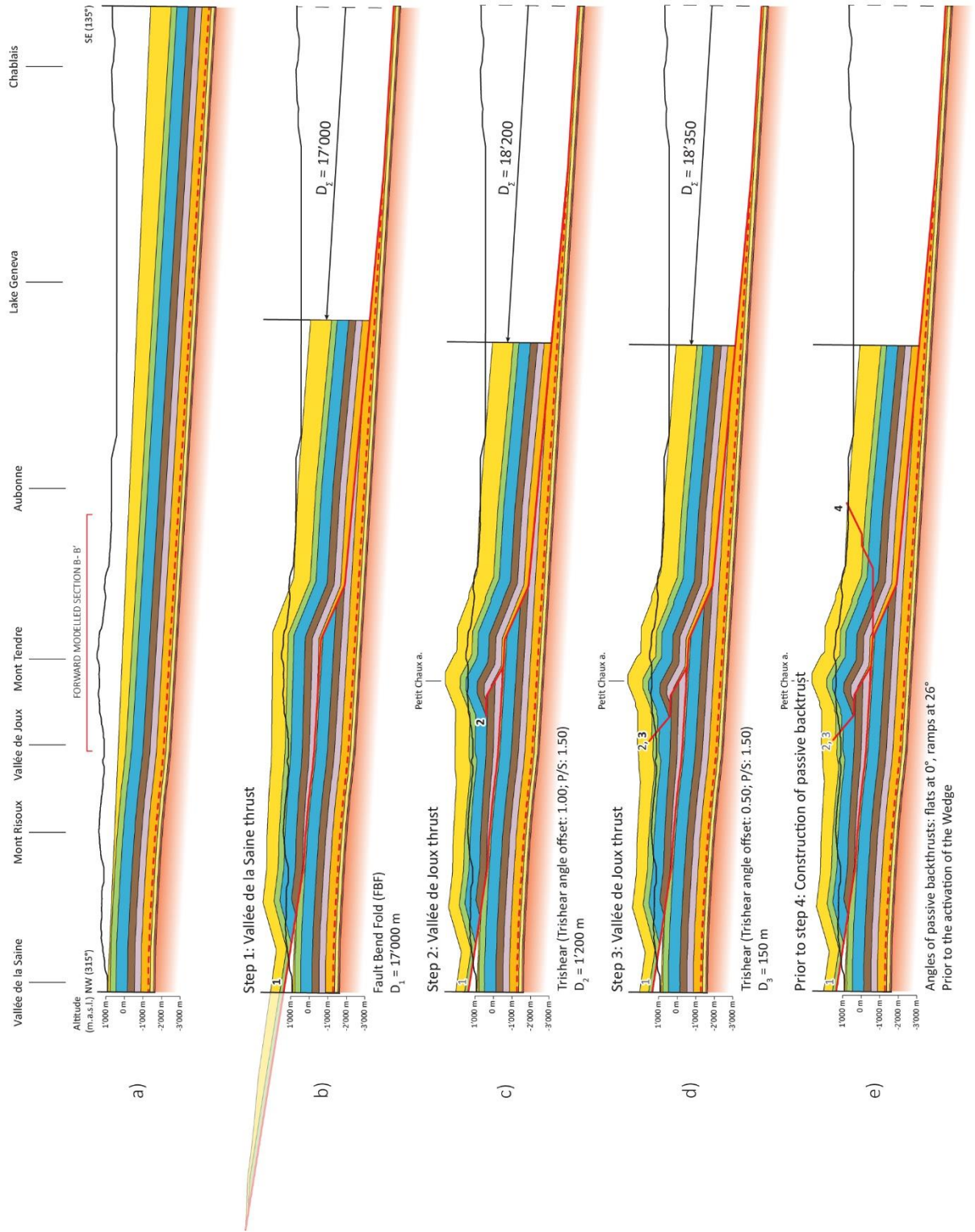
428 2012; Cardozo and Allmendinger 2013). The dip data from fieldwork (N = 799) are presented in a single lower
429 hemisphere stereoplot (Schmidt net: equal area projection) (b). The poles to bedding planes stereoplot is
430 represented using the “Kamb contouring” method. The calculated best fit orientation of the cross-section is 136°
431 $- 316^\circ$, which corresponds to the red line. The red rectangles (N = 8) represent the calculated fold axes of this
432 study. The geological cross-section A – A' runs from the Molasse Basin in Switzerland, through the Mont Tendre
433 and Mont Risoux anticlines to the Vallée de la Saine in France (c). The top crystalline basement's geometry is
434 based on Schori (2021) (figure 6) and the stratigraphic thicknesses correspond to the values indicated in figure 3
435 (A – A'). The surface geology and shallow subsurface structures are defined by the data from fieldwork. The
436 important outcropping thrusts and folds are labelled with a name. The subsurface interpretation is based on the
437 log of the Risoux-1 deep well (appendix 1) and the interpretation of the seismic profiles (figure 5). The section
438 from the Molasse Basin to the Vallée de Joux is marked in red and has been forward modelled to verify its
439 sequence and balancing.

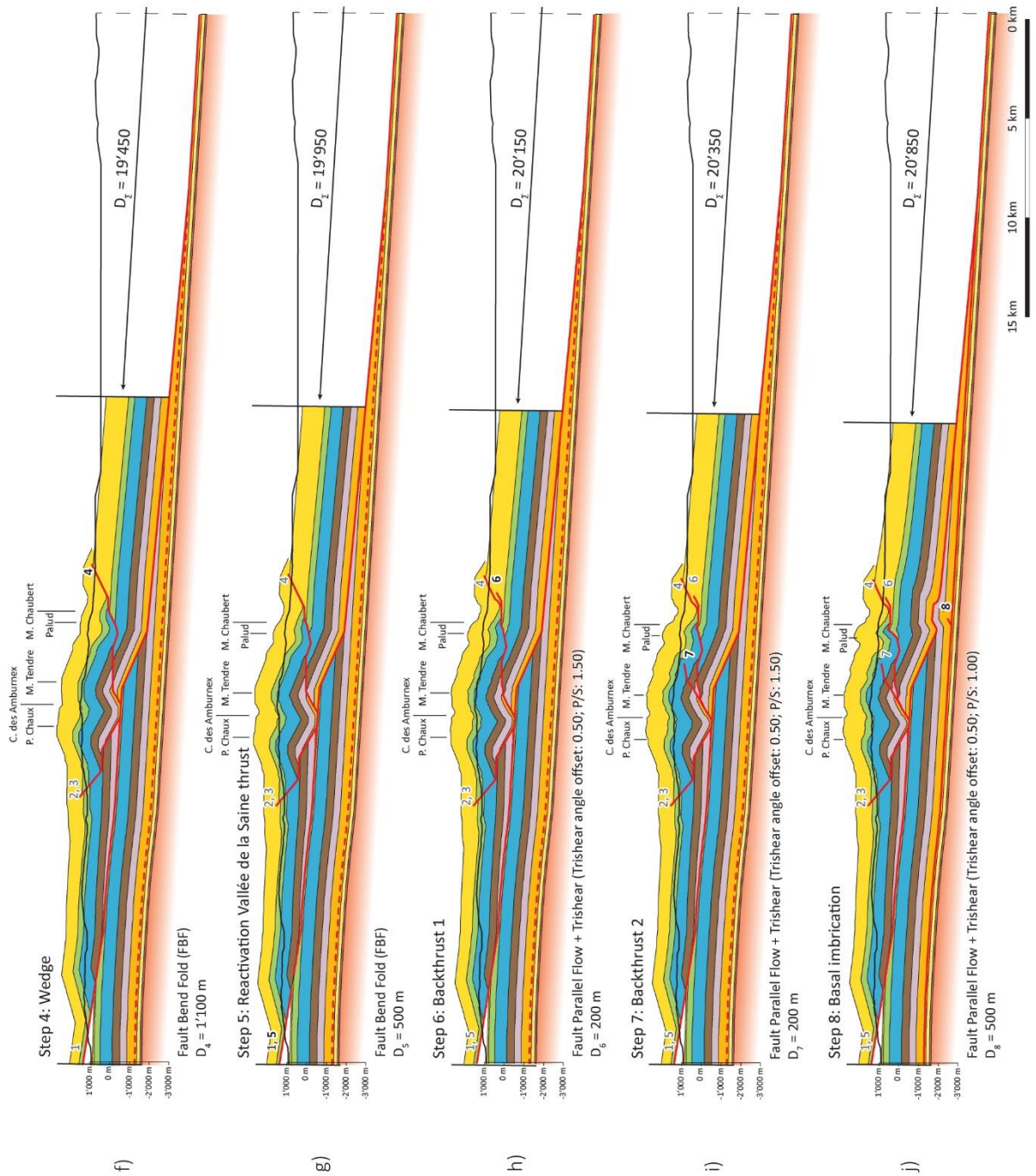
440 5.3 2D kinematic forward model B – B'

441 A 2D kinematic forward modelled section B – B' is proposed for the Mont Tendre anticline s.l. that helps
442 establish a chronology of thrust development on a regional scale and validate the deep subsurface
443 structures. This model is combined with the Mont Risoux anticline s.l. of the geological cross-section
444 to propose a regionally consistent section. The 2D forward model is created by an iterative approach
445 resulting in the most probable modelling sequence (steps a) to j), figures 8 and 9). The applied technical
446 parameters, indicated beneath each modelling step in figures 8 and 9, are those that led to one possible
447 solution and are the result of numerous iterations to best comply with the outcropping geology. The
448 development of a 2D kinematic forward model for the whole NAFB to the Vallée de la Saine syncline
449 was beyond the scope of this project due to the significant additional expense required to develop a
450 forward model for the northern part of the study area. The deformation style for balancing and forward
451 modelling is defined as thrust-related folding and thin-skinned deformation without involvement of the
452 crystalline and mechanical basement. The main basal décollement level was constructed as a smooth
453 plane at the base of the Keuper Group for simplification reasons (Gruber 2017; Marro et al. 2023).
454 Although the stratigraphic thicknesses vary in the field, we ensured a balanced forward model by using

455 constant thicknesses (figure 3). We constructed an initial layer cake with the individual thicknesses of
 456 the Mesozoic units on top and parallel to the crystalline basement, which represents the NAF prior to
 457 the folding and thrusting of the Jura FTB. The top of the Tertiary sediments shows an angle of 2.5°
 458 which is smaller than that of the underlying Mesozoic cover, as it represents the top of the NAFB
 459 sediment wedge. The activation of the basal décollement level is not considered as a separate
 460 modelling step because it does not influence in this study the final structure of the forward model of
 461 the Mont Risoux-Mont Tendre structure (a in figure 8). The formation of the Vallée de la Saine thrust
 462 (FBF), which roots in the basal décollement level, generates a shortening of 17 km and the duplication
 463 of almost the entire post-Triassic cover. The 15 km flat within the marly layers of the Vuache Formation
 464 of Cretaceous age indicates that this is the main regional thrust of this study, other than the basal
 465 décollement level. It thrusts the Liassic units beneath the Mont Risoux anticline (b) (appendix 1). The
 466 Vallée de Joux thrust, is modelled using the trishear algorithm to create the minor Petit Chaux anticline
 467 of the Mont Tendre anticline (c and d). The significance of the backthrusts towards the hinterland is
 468 demonstrated by the wedge modelling that results in the alternating sequence of the minor synclines
 469 and anticlines of the Mont Tendre anticline (e and f) (chapter 4.5 for further information regarding the
 470 wedge modelling). The reactivation of the Vallée de la Saine thrust (g), along with the two backthrusts
 471 rooted in the wedge forming backthrust (h and i) as well as a hinterland-oriented basal imbrication
 472 rooted in the main décollement level (j) steepens the fold limbs and accentuates the minor synclines
 473 and anticlines. Figures 8 and 9 indicate the shortening amounts for each incremental deformation step.
 474 The total shortening (folding and displacement) for the Mont Tendre anticline s.l. is 20.85 km.

475 **Figure 8:** Deformation steps 1 – 4 of the 2D kinematic forward model B – B' from the Molasse Basin to the Vallée
 476 de Joux. The forward model and kinematically balanced cross-section were constructed from the initial layer cake
 477 (a) to the final forward model of this work (j). The basal main décollement level at the base of the Keuper unit is
 478 presented as the red dashed line. The stratigraphic thicknesses used for the forward model are indicated in figure
 479 3 and the legend of the stratigraphy is shown in figure 12. The technical parameters (D_{1-4}) and displacement
 480 applied to reach each step is shown on the right side (abbreviated as D_{Σ}).





482

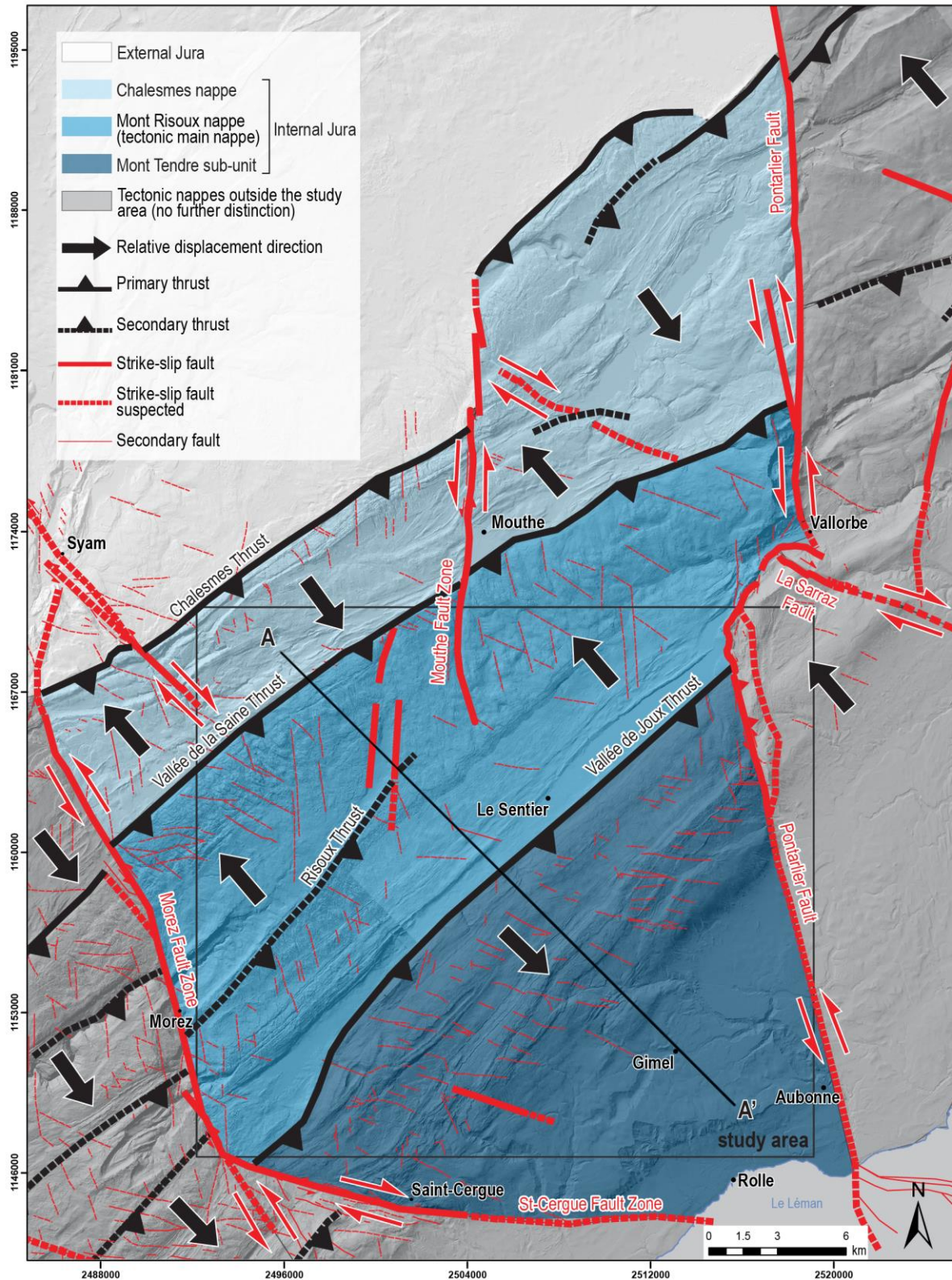
483 **Figure 9:** Deformation steps 4 – 8 of the 2D kinematic forward model B – B' from the Molasse Basin to the Vallée
 484 de Joux. The stratigraphic thicknesses used for the forward model are indicated in figure 3 and the legend of the
 485 stratigraphy is shown in figure 12. The technical parameters (D_{4-8}) and displacement applied to reach each step
 486 is shown on the right side (abbreviated as D_2).

487

488 6 Discussion

489 6.1 Local tectonics

490 The Mont Risoux s.l. and the Mont Tendre s.l. are the two dominant complex anticlinal structures in
491 the study area. Both anticlines together belong to the Mont Risoux nappe, which is linked to the Vallée
492 de la Saine thrust. This thrust accommodated 17 km displacement and led to the duplication of almost
493 the entire Mesozoic unit. The whole area shows a remarkable lateral continuity and cylindricity and
494 therefore we consider that the hanging wall of the Vallée de la Saine thrust forms one tectonic nappe
495 (Marro et al. 2023). The Mont Risoux nappe thrusts towards the northwest on top of the Chalesmes
496 nappe, which in turn thrusts on top of the External Jura. The Mont Tendre nappe, located in the
497 southeast of the study area, is considered to be a sub-unit of the Mont Risoux nappe and consists of a
498 sequence of minor folds. The Mont Risoux nappe is bounded by the Vallée de la Saine thrust and the
499 Vallée de Joux thrust and is laterally limited by the Pontarlier and Morez – St-Cergue strike-slip fault
500 zones (figure 10) (Aubert 1971). These sedimentary cover nappes are generally transported towards
501 the northwest. Depending on the sense of movement of the strike-slip faults, these nappes exhibit
502 relative displacement towards the northwest or southeast (as indicated by the bold black arrows in
503 figure 10), perpendicular to the thrust axes and fold axial traces. The large regional strike-slip faults are
504 arranged in a conjugate setting and therefore indicate the general direction of transport, which
505 coincidentally is perpendicular to the cylindrically major folds and indicate the relative movement of
506 each nappe (see also Marro et al. 2023; Hauvette 2024).



507

508 **Figure 10:** Kinematic map of the local Internal Jura showing the study area and the geological cross-section A –
 509 A'. The fine red lines represent the secondary faults (modified after Sturny 2018 and Schori 2021). The thick red
 510 lines are the primary strike-slip faults that dissect the primary thrusts (modified after Schori 2021). The Internal
 511 Jura is divided into individual sedimentary nappes by primary strike-slip faults and primary thrusts, which limit it

512 laterally and frontally, respectively (indicated in different surface colours). The relative displacement direction of
513 each nappe is shown by black arrows.

514 6.2 Final cross-section and its validated deep structures

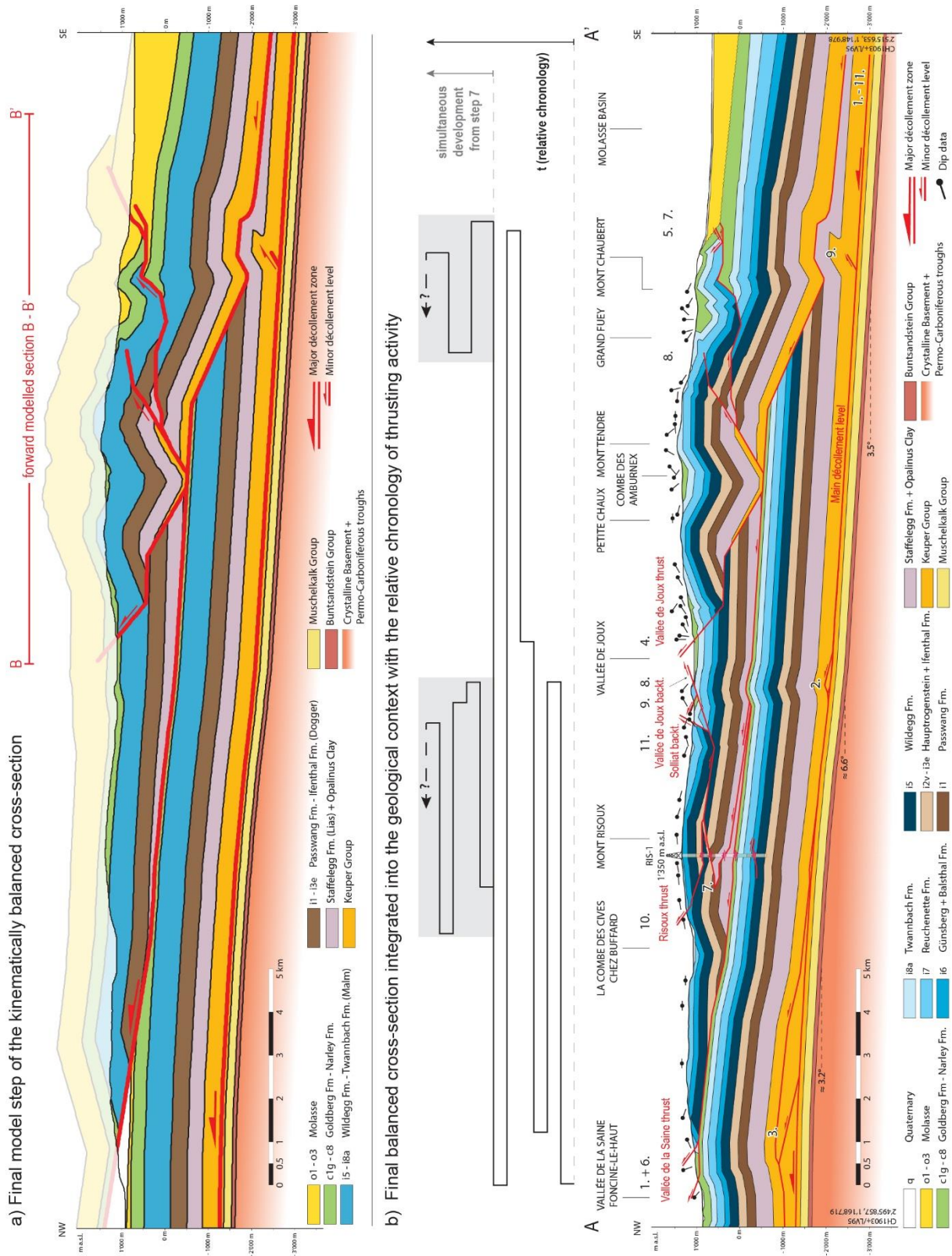
515 This study presents a new cross-section of the Mont Tendre and Mont Risoux anticlines s.l. The surface
516 geology was determined by field observations, remote sensing and geological mapping. The deep
517 surface structures were determined using the near-top crystalline basement (Schori 2021), the
518 description of the Risoux-1 deep well (Winnock 1961), the interpretation of seismic profiles
519 (Sommaruga 1997) and cross-sections from published works. The basal décollement was located at the
520 base of the Keuper Group (see also Sommaruga et al. 2017; Marro et al. 2023). While some authors,
521 such as Bitterli (1972) and Otto (1994), assume a thick-skinned deformation of the central Jura FTB, we
522 propose a pure thin-skinned deformation along the basal décollement level in the Triassic sediments.
523 This is consistent with the cross-sections of Wildi and Huggenberger (1993), Bitterli (1972), Philippe
524 (1995) and Philippe et al. (1996). Wildi and Huggenberger (1993) and Bitterli (1972) propose an
525 uninterpreted subsurface architecture, while Philippe (1995) and Philippe et al. (1996) suggest that two
526 major ramps are rooted in the basal décollement for the formation of the Mont Risoux anticline
527 (appendix 2). However, the seismic interpretations show a package of continuous, horizontal seismic
528 horizons above the crystalline basement, below the Risoux-1 deep well, making it unlikely that ramps
529 exist between the horizontal reflectors (figure 5). The small oblique reflectors further south under the
530 Vallée de Joux syncline are part of a minor fold developed due to late imbrication in the Triassic
531 décollement level (as discussed prior). In light of these data, we propose a solution with single flat
532 detachment linked to one ramp, located below the Mont Tendre anticline, which results in the main
533 regional Vallée de la Saine thrust (figure 7, 11). We propose that the Vallée de la Saine thrust thrusts
534 well identified Liassic units (from borehole data) on top of the Cretaceous units. The presence of clay
535 rich horizons of Cretaceous age appears required to host such a large thrust. Although no Cretaceous
536 series have been formally identified in the log of the Risoux-1 deep well, at a depth of 1234 to 1240 m
537 an important fault is identified. This zone contains breccias of limestone as well as clay rich layers, and

538 microfossils that suggest Upper Jurassic to Lower Cretaceous age (Winnock 1961) corroborating the
 539 likely presence of Cretaceous series. Thus, we propose that the major Vallée de la Saine thrust is rather
 540 situated in the marly layers of the Vuache Formation, than in the massive limestones of the Malm unit
 541 (figure 7 – 9, 11, appendix 1). The Risoux-1 deep well indicates the presence of the Liassic and the
 542 absence of the Keuper units beneath the Mont Risoux anticline. The interpreted seismic profiles show
 543 the additional presence of the Keuper unit beneath the Mont Tendre anticline. Therefore, we propose
 544 that the Keuper unit is tectonically cut off and pinching out between the Mont Tendre anticline and the
 545 Risoux-1 deep well (figure 5, appendix 1). Unlike the solution with several imbricates (e.g. Philippe et
 546 al. 1996 in appendix 2) we tried to acknowledge the presence of all the thrusts described in the Risoux-
 547 1 deep well by proposing a thrust structure with a fishtail geometry with two imbricate wedges in the
 548 upper part of the well, one major décollement in the Lower Cretaceous series and one minor intra-
 549 Malm thrust. Based on the thickness of the series observed in the well, we propose a kinematically
 550 viable solution, although not completely balanced (a fully balanced section would require re-assessing
 551 the borehole data for ages and thicknesses, and is beyond the scope of this paper).

552 We propose a new kinematically balanced forward modelled cross-section of the Mont Tendre anticline
 553 s.l. (figure 11a). The validated deep structures are integrated into the geological cross-section (figure
 554 7c), providing context for the forward model with the subsurface geology of the entire Mont Risoux
 555 nappe (figure 11b). This study aimed to model the minor folds of the shallow subsurface of the Mont
 556 Tendre anticline s.l. using dip data and reliable deep structures. We used a two-step process to model
 557 thrusting towards the hinterland (since there is no proposed solution in MOVE). In a first step the FPF
 558 algorithm is applied towards the foreland with a defined displacement and a subsequent Trishear
 559 algorithm is applied with the same amount of displacement to achieve motion towards the hinterland
 560 and thus remain consistent with the surface data and geometries (for further information, refer to Rime
 561 et al. 2019). Another limitation is the use of constant stratigraphic thicknesses over the entire cross-
 562 section. Indeed, geophysical investigations show that the thickness of the Mesozoic cover varies
 563 constantly in the Jura FTB (Marchant 2016; Gruber 2017; Sommaruga et al. 2017; Schori 2021).

564 Nevertheless, the stratigraphic thickness defined for the geological cross-section A – A' and for the 2D
565 forward modelled section B – B' remains constant along the section traces. The total stratigraphic
566 thickness of the Mesozoic sedimentary rocks is 90 meters thinner for the 2D forward modelled section
567 than for the geological cross-section (figure 3). This ensures the outcrop of the Cretaceous unit at the
568 Mont Chaubert and in the Vallée de Joux in the 2D forward model. The area beneath the Vallée de Joux
569 is therefore a transition zone between the two thicknesses.

570 In conclusion, the final cross-section proposes a relative chronology of thrusting activity, with the Vallée
571 de la Saine thrust being formed first, followed by an oscillating thrust sequence between the Mont
572 Tendre and Mont Risoux anticlines s.l., while the Mont Tendre and Mont Risoux anticline thrust
573 sequences developed simultaneously. This leads to a new interpretation of the subsurface geology of
574 the local Internal Jura FTB (figure 11b).



575

576 **Figure 11:** Comparison of the final model step of the kinematically balanced cross-section B – B' (a) with the final
 577 cross-section A – A' (b) of this study. The geological cross-section extends from the Vallée de Joux to the Vallée
 578 de la Saine and contextualises the forward model B – B', which ranges from the Molasse Basin to the Vallée de
 579 Joux. The numbers indicate the chronology of the thrust development at a regional scale and propose a relative

580 chronology of the thrusting activity. The stratigraphic thicknesses used for the forward model are indicated in
581 figure 3 (B – B'), while those of the northern section correspond to the values indicated in figure 3 (A – A').

582

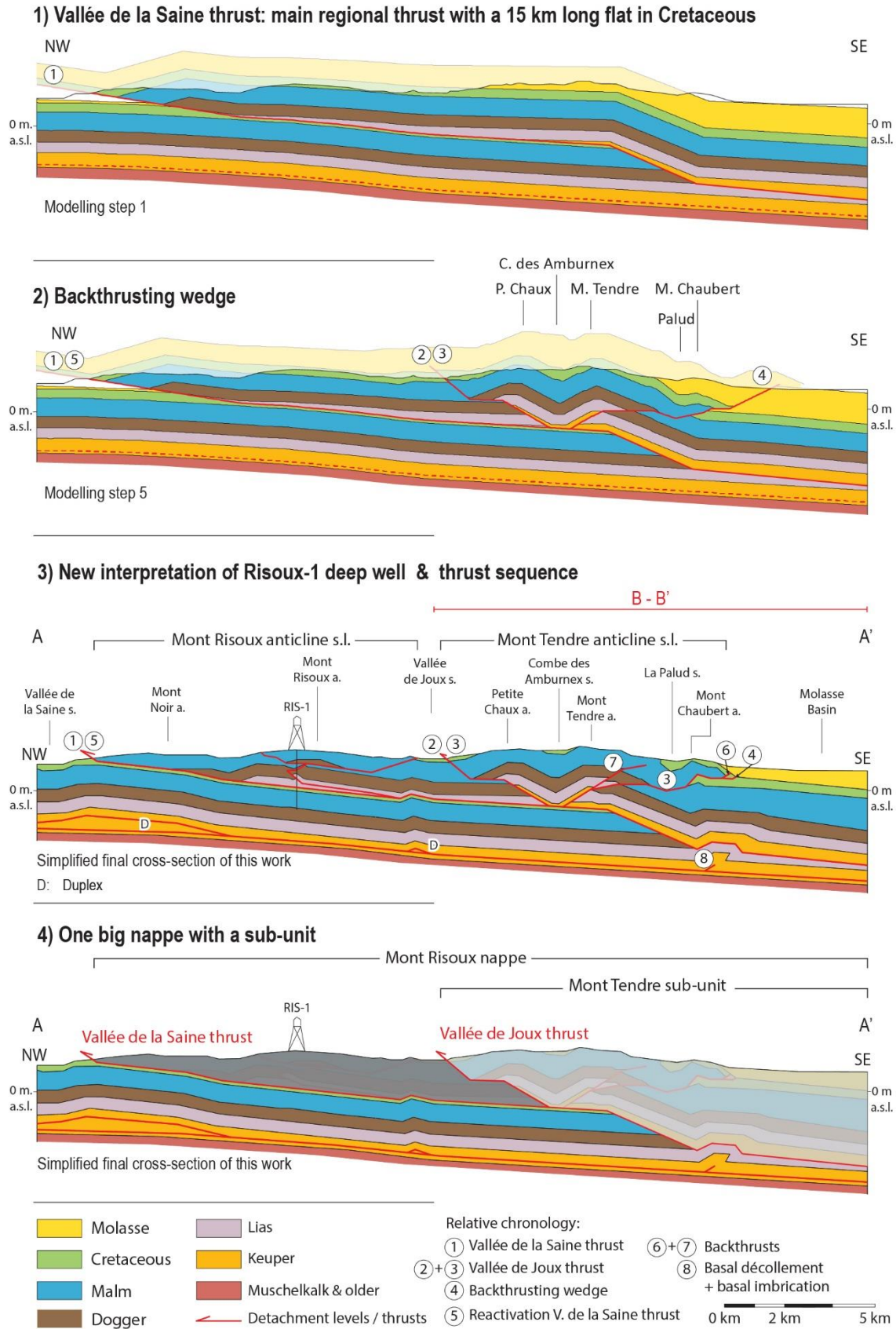
583 7 Conclusion

584 Based on fieldwork, remote sensing and data compilation of previous studies and geological maps, we
585 present a new structural model of the Mont Tendre and Mont Risoux anticlines s.l. situated in the
586 Internal Jura FTB (figure 12). We propose a refined understanding of the wedge geometry, especially in
587 relation to the local, subsurface geology in context of the near-top basement surface (Schori 2021), as
588 well as the identification of a large-scale structural tectonic unit, the Mont Risoux nappe, with an
589 important lateral continuity, formed by the main regional Vallée de la Saine thrust. The thrust has a 15
590 km long flat in the Cretaceous units and accommodates a displacement of 17 km. The activation of the
591 Vallée de Joux thrust resulted in the formation of the Mont Tendre anticline s.l. leading to the dissection
592 of the Mont Risoux nappe into a sub-unit to the SE, the Mont Tendre nappe. The Vallée de Joux thrust
593 was followed by a backstepping sequence and a locally oscillating thrust sequence, resulting in a
594 complex kinematic sequence. This detailed interpretation of the sequential development, highlighting
595 the importance of top to the south thrusting (backthrusting), confirms the mechanics of a low-tapered
596 wedge with the décollement in the weak evaporites promoting backthrusting.

597 These tectonic nappes demonstrate the lateral structural subdivision by first order thrusts, which have
598 a NE – SW orientation, and by first order strike-slip faults, which have a NNW – SSE and ESE – WNW
599 orientation (figure 10).

600 The interpretation of the Risoux-1 deep well has led to the determination of the significant secondary
601 décollement levels in the clay-rich Lower to Middle Jurassic series that lead to the formation of
602 important flats, fishtail and pop-up geometries in structurally higher levels. The importance of major
603 thrusting in the clay-rich Middle Cretaceous series is recognised as a corollary of the structural
604 modelling.

605 We hereby propose a kinematically viable solution for the activation of the Vallée de la Saine thrust
606 and the formation of the Mont Tendre anticline, which were active between 14 Ma and 4 Ma and
607 accommodated a shortening of 20.85 km.



608

609 **Figure 12:** The first modelling step highlights the importance of the 15 km long flat of the Vallée de la Saine thrust

610 and the formation of the Mont Risoux nappe (1). The fifth modelling step highlights the backthrusting wedge that

611 shapes the Mont Tendre anticline (2). The final cross-section underlines, although simplified, the relative
612 chronology of the thrust development of the Mont Tendre anticline s.l. (s. = syncline, a. = anticline) (3). The study
613 area consists of the Mont Risoux nappe, which includes the Mont Tendre sub-unit (4).

614

615 **Declarations**

616 Availability of data and materials

617 The datasets used and/or analysed during the current study are available from the corresponding
618 author on reasonable request.

619 Competing interests

620 The authors declare that they have no competing interests.

621 Funding

622 This work has been funded by the University of Fribourg.

623 Authors' contributions

624 AU conducted the fieldwork, constructed the geological cross-section, performed the forward
625 modelling in MOVE, prepared the figures and wrote this manuscript. JM accompanied AU in the field,
626 completed and improved this text, and provided support at all stages of this study. The authors
627 discussed the results and reviewed this article. The final manuscript was read and approved by both
628 authors.

629 Acknowledgements

630 We would like to thank Sandra Borderie for her assistance during fieldwork, Marc Schori for his research
631 results, Anna Sommaruga for providing her interpreted seismic lines, Adeline Marro and Valentin Rime
632 for discussions and recommendations on the MOVE software. We thank Petroleum Experts for
633 providing the MOVE software, which was used for the forward modelling.

634 **References**

- 635 Allmendinger RW, Cardozo N, Fisher D (2012) Structural geology algorithms: Vectors and tensors in
636 structural geology. Cambridge University Press.
- 637 Aubert D (1941) Vallée de Joux (AS 288, 297 bis - 299, La Muratte - Les Mines - Le Lieu - Le Brassus – Le
638 Sentier, CN 1221 Le Sentier) avec annexes des feuilles 291 Vallorbe et 300 Mont-la-Ville. In: Geological
639 Atlas of Switzerland 1:25000. Vol. 17. Wabern, Switzerland: Federal Office of Topography (swisstopo).
- 640 Aubert D (1945) Le Jura et la tectonique d'écoulement. Mémoires de la Société Vaudoise des Sciences
641 Naturelles 8(4): 217–236.
- 642 Aubert, D. (1959) Le décrochement de Pontarlier et l'orogénèse du Jura. Mémoires de la Société
643 Vaudoise des Sciences Naturelles, 12(4): 93–152.
- 644 Aubert D, Dreyfuss M (1963) Orbe (CN 1202). In: Geological Atlas of Switzerland 1:25000. Vol. 42.
645 Wabern, Switzerland: Federal Office of Topography (swisstopo).
- 646 Aubert D (1971) Le Risoux, un charriage jurassien de grandes dimensions. *Eclogae Geologicae Helvetiae*
647 64(1): 152–156. <https://doi.org/10.5169/seals-163975>
- 648 Becker A (2000) The Jura Mountains — an active foreland fold-and-thrust belt? *Tectonophysics* 321(4):
649 381–406. [https://doi.org/10.1016/S0040-1951\(00\)00089-5](https://doi.org/10.1016/S0040-1951(00)00089-5)
- 650 Bitterli P (1972) Erdölgeologische Forschungen im Jura. *Bulletin der Vereinigung Schweiz. Petroleum-*
651 *Geologen und -Ingenieure* 39: 13–28.
- 652 Boyer S, Elliott D (1982) Thrust systems. *American Association of Petroleum Geologists Bulletin* 66(9):
653 1196–1230.
- 654 BRGM (2020) InfoTerre <http://infoterre.brgm.fr/viewer/MainTileForward.do> [Accessed on 28.10.2021]
- 655 Burg JP (2018) Script to Structural Geology. Eidgenössische Technische Hochschule Zürich ETH
656 Geologisches Institut Zürich. <https://doi.org/10.3929/ethz-b-000279493>

- 657 Burkhard M, Sommaruga A (1998) Evolution of the western Swiss Molasse basin: Structural relations
658 with the Alps and the Jura belt. *Geological Society London Special Publications* 134: 279–298.
659 <https://doi.org/10.1144/gsl.sp.1998.134.01.13>
- 660 Buxtorf A (1907) Zur Tektonik des Kettenjura. *Bericht der Versammlung des Oberrheinischen*
661 *Geologischen Vereins* 40: 29–38.
- 662 Buxtorf A (1916) Prognosen und Befunde beim Hauensteinbasis- und Grenchenbergtunnel und die
663 Bedeutung der Letzteren für die Geologie des Juragebirges. *Verhandlungen der Naturforschenden*
664 *Gesellschaft in Basel* 27: 184–254.
- 665 Cardozo N, Allmendinger RW (2013) Spherical projections with OSXStereonet. *Computers &*
666 *Geosciences* 51: 193–205. <https://doi.org/10.1016/j.cageo.2012.07.021>
- 667 Custer W, Aubert, D (1935) Cossonay (CN 1222). In: *Geological Atlas of Switzerland* 1:25000. Vol. 5.
668 Wabern, Switzerland: Federal Office of Topography (swisstopo).
- 669 Davis D, Engelder, T (1985) The role of salt in fold-and-thrust belts. *Tectonophysics* 119(1–4): 67–88.
670 [https://doi.org/10.1016/0040-1951\(85\)90033-2](https://doi.org/10.1016/0040-1951(85)90033-2)
- 671 DeCelles PG, Giles KA (1996) Foreland basin systems. *Basin Research* 8(2): 105–123.
672 <https://doi.org/10.1046/j.1365-2117.1996.01491.x>
- 673 Deville E, Blanc E, Tardy M, Beck C, Cousin M, Ménard G (1994) Thrust Propagation and Syntectonic
674 Sedimentation in the Savoy Tertiary Molasse Basin (Alpine Foreland). In: Mascle, A. (Eds) *Hydrocarbon*
675 *and Petroleum Geology of France. Special Publication of the European Association of Petroleum*
676 *Geoscientists* (vol 4: 269–280). Springer Berlin Heidelberg. [https://doi.org/10.1007/978-3-642-78849-](https://doi.org/10.1007/978-3-642-78849-9_19)
677 [9_19](https://doi.org/10.1007/978-3-642-78849-9_19)
- 678 Deville E, Sassi W (2006) Contrasting thermal evolution of thrust systems: An analytical and modeling
679 approach in the front of the western Alps. *American Association of Petroleum Geologists Bulletin* 90(6):
680 887–907. <https://doi.org/10.1306/01090605046>

- 681 Deville E (2021) Structure of the Tectonic Front of the Western Alps: Control of Fluid Pressure and Halite
682 Occurrence on the Decollement Processes. *Tectonics* 40. <https://doi.org/10.1029/2020TC006591>
- 683 Egan SS, Buddin TS, Kane S, Williams GD (1997) Three-dimensional modelling and visualisation in
684 structural geology: new techniques for the restoration and balancing of volumes. In: Proceedings of
685 the 1996 Geoscience Information Group Conference on Geological Visualisation *Electronic Geology*
686 Special 1: 67–82.
- 687 Egan SS, Kane S, Buddin T.S, Williams GD, Hodgetts D (1999) Computer modelling and visualisation of
688 the structural deformation caused by movement along geological faults. *Computers & Geosciences*
689 25(3): 283-297.
- 690 Endignoux L, Mugnier JL (1990) The use of a forward kinematic model in the construction of balanced
691 cross sections. *Tectonics* 9(5): 1249–1262. <https://doi.org/10.1029/TC009i005p01249>
- 692 Erslev EA (1991) Trishear fault-propagation folding. *Geology* 19(6): 617–620.
- 693 Falconnier A (1950) Marchairuz (CN 1241). In: *Geological Atlas of Switzerland 1:25'000*. Vol. 25.
694 Wabern, Switzerland: Federal Office of Topography (swisstopo).
- 695 Fossen H (2010) *Structural Geology*. 1st edn. Cambridge University Press, 463 pp.
- 696 Goguel J (1952) *Traité de tectonique*. Masson Paris.
- 697 Gruber M (2017) *Structural Investigations of the Western Swiss Molasse Basin - From 2D Seismic*
698 *Interpretation to a 3D Geological Model*. PhD thesis, Université de Fribourg, Fribourg, Switzerland. 190
699 pp.
- 700 Hauvette L (2024) *Tectonics of the Western North Alpine Foreland based on seismic interpretation of*
701 *the Greater Geneva Basin*. PhD thesis, Université de Fribourg, Fribourg, Switzerland. 270 pp.
702 <http://doi.org/10.51363/unifr.sth.2024.009>

- 703 Homberg C, Lacombe O, Angelier J, Bergerat F (1999) New constraints for indentation mechanisms in
704 arcuate belts from the Jura Mountains, France. *Geology* 27(9): 827–830. [https://doi.org/10.1130/0091-7613\(1999\)027%3C0827:NCFIMI%3E2.3.CO;2](https://doi.org/10.1130/0091-7613(1999)027%3C0827:NCFIMI%3E2.3.CO;2)
- 706 Homberg C, Bergerat F, Philippe Y, Lacombe O, Angelier J (2002) Structural inheritance and Cenozoic
707 stress fields in the Jura fold-and-thrust belt (France). *Tectonophysics* 357(1–4): 137–158.
708 [https://doi.org/10.1016/S0040-1951\(02\)00366-9](https://doi.org/10.1016/S0040-1951(02)00366-9)
- 709 Hossack JR (1979) The use of balanced cross section in the calculation of orogenic contraction, a review.
710 *Journal of the Geological Society London* 136: 705-711. <https://doi.org/10.1144/gsjgs.136.6.0705>
- 711 IGN-F (2018) MNT RGE ALTI 5m Digital Elevation Models. Institut national de l'information
712 géographique et forestière (IGN-F). <http://www.ign.fr>. [Accessed on 04.01.2022]
- 713 Jordan P (1992) Evidence for large-scale decoupling in the Triassic evaporites of northern Switzerland:
714 An overview. *Eclogae Geologicae Helvetiae* 85(3): 677–693. <https://doi.org/10.5169/seals-167025>
- 715 Kane SJ, Williams GD, Buddin TS, Egan SS, Hodgetts D (1997) Flexural-slip based restoration in 3D, a
716 new approach. *American Association of Petroleum Geologists Bulletin Annual Convention Official*
717 *Program*: A58.
- 718 Kuhlemann J, Kempf O (2002) Post-Eocene evolution of the North Alpine Foreland Basin and its
719 response Alpine tectonics. *Sedimentary Geology* 152: 45–78. [https://doi.org/10.1016/S0037-0738\(01\)00285-8](https://doi.org/10.1016/S0037-0738(01)00285-8)
- 721 Laubscher HP (1961) Die Fernschubhypothese der Jurafaltung. *Eclogae Geologicae Helvetiae* 54(1):
722 222–282. <https://doi.org/10.5169/seals-162820>
- 723 Laubscher HP (1965) Ein kinematisches Modell der Jurafaltung. *Eclogae Geologicae Helvetiae* 58(1):
724 232–318. <https://doi.org/10.5169/seals-163266>
- 725 Laubscher HP (1972) Some overall aspects of Jura dynamics. *American Journal of Science* 272: 293–
726 304. <https://doi.org/10.2475/ajs.272.4.293>

- 727 Laubscher HP (2008) The Grenchenberg conundrum in the Swiss Jura: A case for the centenary of the
728 thin-skin décollement nappe model (Buxtorf 1907). *Swiss Journal of Geosciences* 101: 41–60.
729 <https://doi.org/10.1007/s00015-008-1248-2>
- 730 Lithostratigraphic Lexicon of Switzerland (2021). Online Lexicon strati.ch. www.strati.ch [Accessed on
731 21.12.2021]
- 732 Madritsch H, Looser N, Schneeberger R, Wohlwend S, Guillong M, Malz A (2024) Reconstructing the
733 Evolution of Foreland Fold-And-Thrust Belts Using U-Pb Calcite Dating: An Integrated Case-Study From
734 the Easternmost Jura Mountains (Switzerland). *Tectonics* 43. <https://doi.org/10.1029/2023TC008181>
- 735 Marchant R (2016) GeoMol-Vaud final report. Musée Cantonal de Géologie Direction Générale de
736 l’environnement (DGE) Géologie, sols et déchets, Canton de Vaud, Switzerland, 79 pp.
- 737 Marro A, Hauvette L, Borderie S, Mosar J (2023) Tectonics of the Western Internal Jura fold-and-thrust
738 belt: 2D kinematic forward modelling. *Swiss Journal of Geosciences* 116: 10.
739 <https://doi.org/10.1186/s00015-023-00435-2>
- 740 Mitra S (1986) Duplex structures and imbricate thrust systems: Geometry, structural position, and
741 hydrocarbon potential. *American Association of Petroleum Geologists Bulletin* 70: 1087–1112.
742 <http://doi.org/10.1306/94886A7E-1704-11D7-8645000102C1865D>
- 743 Mosar J (1999) Present-day and future tectonic underplating in the western Swiss Alps: Reconciliation
744 of basement/wrench-faulting and décollement folding of the Jura and Molasse basin in the Alpine
745 foreland. *Earth and Planetary Science Letters* 173(3): 143–155. [https://doi.org/10.1016/S0012-
746 821X\(99\)00238-1](https://doi.org/10.1016/S0012-821X(99)00238-1)
- 747 Mosar J, Borderie S, Hauvette L, Marro A (2025a) Stress in the Greater Geneva Basin. *Swiss Journal of*
748 *Geosciences*. 118: 10. <http://doi.org/10.1186/s00015-025-00482-x>
- 749 Mosar J, Schori M, Borderie S, Marro A, Sommaruga A (2025b) Tectonique de socle et Prisme
750 mécanique dans le Jura. *Terre et Sciences* n°2 : 38-45.

- 751 Nussbaum C, Kloppenburg A, Caër T, Bossart P (2017) Tectonic evolution around the Mont Terri rock
752 laboratory, northwestern Swiss Jura: Constraints from kinematic forward modelling. *Swiss Journal of*
753 *Geosciences*, 110: 39–66. https://doi.org/10.1007/978-3-319-70458-6_3
- 754 Otto S (1994) Bresse-Valence Basin & Jura Fold belt. Basin Monitor Group, Petroconsultants (UK).
- 755 Pfiffner OA, Schlunegger F, Buiter SJH (2002) The Swiss Alps and their peripheral foreland basin:
756 Stratigraphic response to deep crustal processes. *Tectonics* 21(2): 1–15.
757 <http://doi.org/10.1029/2000TC900039>
- 758 Pfiffner OA (2010) *Geologie der Alpen*. 2., korrigierte Auflage, Haupt, Bern. 360 pp.
- 759 Philippe Y (1995) Rampes latérales et zones de transfert dans les chaînes plissées: géométrie,
760 conditions de formation et pièges structuraux associés. PhD thesis. Université de Savoie, France. 158
761 pp.
- 762 Philippe Y, Colletta B, Deville E, Mascle A (1996) The Jura fold-and thrust belt: A kinematic model based
763 on map-balancing. *Mémoires du Muséum National d'histoire Naturelle* 1993(170) : 235–261.
- 764 Radaideh OMA, Mosar J (2019) Tectonics controls on fluvial landscapes and drainage development in
765 the westernmost part of Switzerland: Insights from DEM-derived geomorphic indices. *Tectonophysics*
766 768: 228179. <http://dx.doi.org/10.1016/j.tecto.2019.228179>
- 767 Rigassi D (1962) A propos de la tectonique du Risoux. *Bulletin Vereinigung Schweizer Petroleum-*
768 *Geologen und Ingenieuren*, 29/76, 39-50.
- 769 Rigassi D (1977) Encore le Risoux. *Bulletin de la Société vaudoise des naturelles*, 73, 379-413.
- 770 Rime V (2018) Tectonics of the Neuchâtel Jura Mountains. Insight from mapping and forward
771 modelling. Master thesis, University of Fribourg, Fribourg, Switzerland. 156 pp. Unpublished.

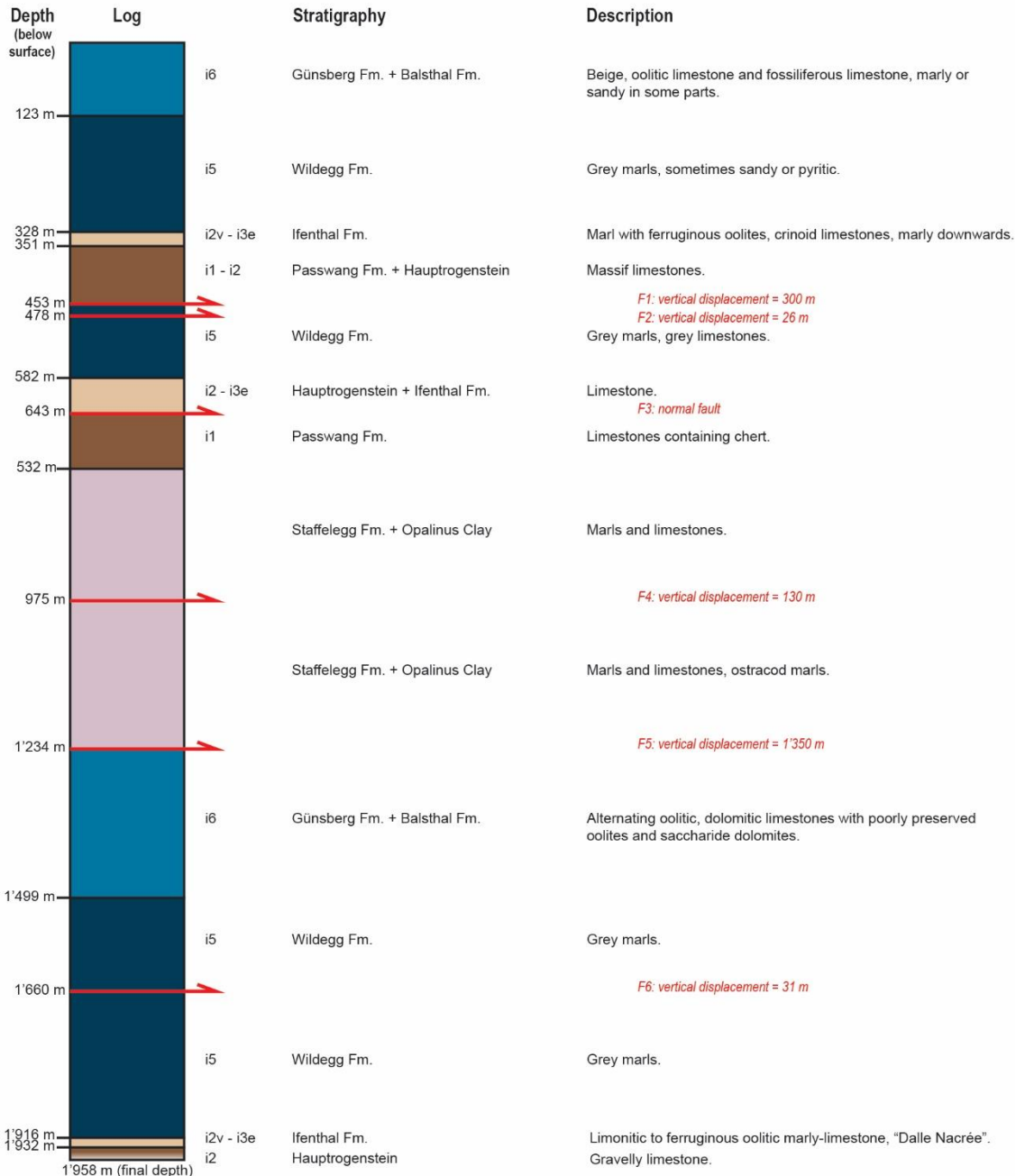
- 772 Rime V, Sommaruga A, Schori M, Mosar J (2019) Tectonics of the Neuchâtel Jura Mountains: Insights
773 from mapping and forward modelling. *Swiss Journal of Geosciences* 112: 563–578.
774 <http://dx.doi.org/10.1007/s00015-019-00349-y>
- 775 Schlunegger F, Mosar J (2011) The last erosional stage of the Molasse Basin and the Alps. *Journal of*
776 *Earth Sciences* 100(5): 1147–1162. <http://dx.doi.org/10.1007/s00531-010-0607-1>
- 777 Schori M (2014) Combined structural field investigations and remote sensing analysis of the Combe
778 Grède area (Chasseral, Central Jura). Master thesis, University of Bern, Bern, Switzerland. Unpublished.
- 779 Schori M, Mosar J, Schreurs G (2015) Multiple décollements during thin-skinned deformation of the
780 Swiss Central Jura: A kinematic model across the Chasseral. *Swiss Journal of Geosciences* 108: 327–
781 343. <http://doi.org/10.1007/s00015-015-0196-x>
- 782 Schori M (2021) The development of the Jura fold-and-thrust belt: Pre-existing basement structures
783 and the formation of ramps. PhD thesis. Université de Fribourg, Fribourg, Switzerland. 200 pp.
784 <http://doi.org/10.51363/unifr.sth.2022.001>
- 785 Smeraglia L, Looser N, Fabbri O, Choulet F, Guillong M, Bernasconi S (2021) U-Pb dating of middle
786 Eocene-middle Pleistocene multiple tectonic pulses in the Alpine foreland. In: *Solid Earth Discussions*
787 12: 2539–2551. <http://doi.org/10.5194/se-12-2539-2021>
- 788 Sommaruga A (1997) Geology of the Central Jura and the Molasse Basin: New insight into an evaporite-
789 based foreland fold and thrust belt. *Mémoire de la Société Neuchâteloise des Sciences Naturelles* 12:
790 1–176.
- 791 Sommaruga A, Eichenberger U, Marillier, F (2012) Seismic Atlas of the Swiss Molasse Basin. In E. Kissling
792 (Ed.), *Matériaux pour la Géologie de la Suisse—Géophysique*, Federal Office of Topography (swisstopo)
793 44: 90.
- 794 Sommaruga A, Mosar J, Schori M, Gruber M (2017) The Role of the Triassic Evaporites Underneath the
795 North Alpine Foreland. In: JI Soto, J Flinch, G Tari (Eds.), *Permo-Triassic Salt Provinces of Europe*, North

- 796 Africa and the Atlantic Margins. Elsevier, 447–466). [http://dx.doi.org/10.1016/B978-0-12-809417-](http://dx.doi.org/10.1016/B978-0-12-809417-4.00021-5)
797 4.00021-5
- 798 Sturny J (2018) Die Brüche im Faltenjura auf und um den Mont Tendre. Bachelor thesis. Université de
799 Fribourg, Fribourg, Switzerland. 58 pp. Unpublished.
- 800 Suppe J (1983) Geometry and kinematics of fault-bend folding. American Journal of Science, 283: 684–
801 721.
- 802 Swisstopo (2011) Digital elevation model swissALTI3D. Federal Office of Topography (swisstopo),
803 Wabern, Switzerland. www.swisstopo.ch
- 804 Swisstopo (2012) GeoCover-geological vector data. Federal Office of Topography (swisstopo), Wabern,
805 Switzerland. www.map.geo.admin.ch
- 806 Vemet JP (1972) Morges (CN 1242). In: Geological Atlas of Switzerland 1:25'000. Vol. 62. Wabern,
807 Switzerland: Federal Office of Topography (swisstopo).
- 808 Wildi W, Blondel Th, Charollais JJ, Jaquet JM, Wernli R (1991) Tectonique en rampe latérale à la
809 terminaison occidentale de la Haute-Chaîne du
810 Jura. *Eclogae Geologicae Helveticae*, 84(1): 265–277.
- 811 Wildi W, Huggenberger P (1993) Reconstitution de la plate-forme européenne anté-orogénique de la
812 Bresse aux Chaînes subalpines; éléments de cinématique alpine (France et Suisse occidentale). *Eclogae*
813 *Geologicae Helveticae* 86(1) : 47–64.
- 814 Winnock E (1961) Résultats géologiques du forage Risoux 1. Bulletin der Vereinigung Schweizerischer
815 Petroleum-Geologen und Ingenieure 28(74): 17–26. <https://doi.org/10.5169/seals-191403>

RISOUX-1 DEEP WELL

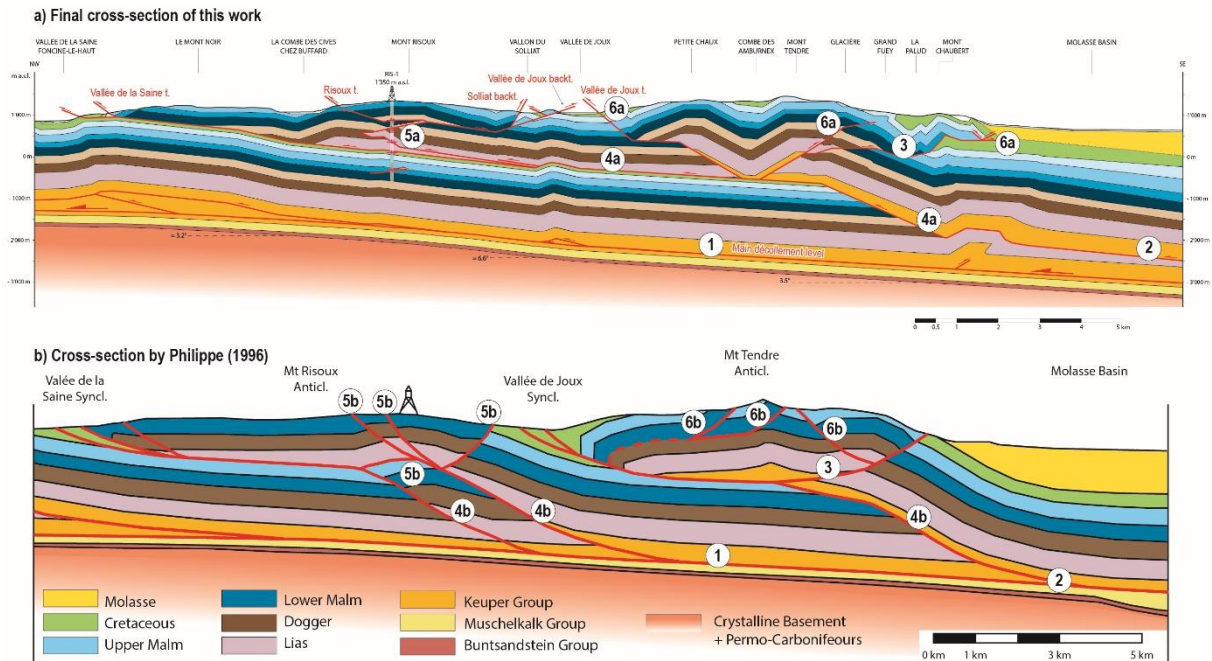
Altitude: 1'350 m a.s.l.
 Coordinates (CH1903+): 2'500'290, 1'161'028

Contracting entity: Prospection et Exploitation Pétrolières
 en Alsace (PREPA) / Canton of Vaud



816

817 **Appendix 1:** Stratigraphic log of the Risoux-1 deep well described by Winnock (1961). The depth of the
 818 stratigraphic limits and faults below the surface are indicated in meters. The stratigraphy is presented with the
 819 corresponding indexes, representing the official formations and groups. The description on the right-hand side is
 820 the translation of the original description in French, which also indicates the amount of displacement per thrust.



821

822 **Appendix 2:** Comparison of the final balanced cross-section (a) with the cross-section from Philippe et al. (1996)
 823 (b). The legend of the stratigraphy is indicated in figure 3 and 12. Both cross-sections propose a thin-skinned
 824 deformation with the basal main décollement level located in the Keuper units (1) and thrust-related folding. The
 825 thrusts consist of ramps and flats, which root in the basal décollement level within the Triassic evaporites (2). The
 826 formation of a wedge (3) occurs in both cases due to the development of a backthrust towards the hinterland.
 827 We propose one main regional Vallée de la Saine thrust with its ramp located beneath the Mont Tendre anticline
 828 (4a). However, Philippe et al. (1996) propose two ramps beneath the Vallée de Joux syncline in addition to a ramp
 829 beneath the Mont Tendre anticline (4b). We propose for the Mont Risoux anticline s.l. a fishtail and pop-up
 830 geometry rooted in the Vallée de la Saine thrust which explain the multiple repetitions of the Mesozoic cover
 831 (5a). Philippe et al. (1996) propose a pop-up geometry formed by two thrusts and a backthrust. We propose for
 832 the formation of the Mont Tendre anticline the Vallée de Joux thrust towards the foreland and two backthrusts
 833 towards the hinterland (6a). In contrast, Philippe et al. (1996) propose two backthrusts and a pop-up geometry
 834 (6b).